



Sales De Freitas, F., Pancost, R., & Arndt, S. (2017). The impact of alkenone degradation on UK'37 paleothermometry: a model-derived assessment. *Paleoceanography*, 32(6), 648. <https://doi.org/10.1002/2016PA003043>

Peer reviewed version

License (if available):
Unspecified

Link to published version (if available):
[10.1002/2016PA003043](https://doi.org/10.1002/2016PA003043)

[Link to publication record in Explore Bristol Research](#)
PDF-document

This is the author accepted manuscript (AAM). The final published version (version of record) is available online via Wiley at <http://onlinelibrary.wiley.com/doi/10.1002/2016PA003043/full> . Please refer to any applicable terms of use of the publisher.

University of Bristol - Explore Bristol Research

General rights

This document is made available in accordance with publisher policies. Please cite only the published version using the reference above. Full terms of use are available:
<http://www.bristol.ac.uk/pure/about/ebr-terms>

1 **The impact of alkenone degradation on $U_{37}^{K'}$ paleothermometry: a model-derived**
2 **assessment**

3 **Felipe S. Freitas**^{1,2,3}, **Richard D. Pancost**^{1,3}, **Sandra Arndt**^{2,3,4}

4 ¹Organic Geochemistry Unit, School of Chemistry, University of Bristol, Bristol, BS8 1TS,
5 UK

6 ²BRIDGE, School of Geographical Sciences, University of Bristol, Bristol, BS8 1SS, UK

7 ³The Cabot Institute, University of Bristol, Bristol, BS8 1UJ, UK

8 ⁴Department of Geosciences, Environment and Society, Université Libre de Bruxelles,
9 Bruxelles 1050, Belgium

10 Corresponding author: Felipe S. Freitas (felipe.salesdefreitas@bristol.ac.uk;

11 +44(0)1173317244)

12
13
14 **Key Points:**

- 15 • Reaction-Transport modelling shows that selective degradation of alkenones can
16 positively bias SST records
- 17 • SST records are only likely to be affected if alkenones experience extensive
18 degradation during burial
- 19 • The majority of alkenone-based SST records are unlikely to be affected by post-burial
20 selective degradation

21
22

23 **Abstract**

24 The $U_{37}^{K'}$ proxy for past sea surface temperature (SST) is based on the unsaturation ratio of C_{37}
25 alkenones. It is considered a diagenetically robust proxy, but biases have been invoked because
26 the index can be altered by preferential degradation of the $C_{37:3}$ alkenone, resulting in higher
27 reconstructed SST. However, alkenone degradation rate constants are poorly constrained,
28 making it difficult to evaluate the plausibility of such a bias. Therefore, we quantitatively
29 assessed the effect of: (1) different alkenone degradation rate constants; (2) differential
30 degradation factors between di- and tri-unsaturated C_{37} alkenones; (3) and initial $U_{37}^{K'}$ values on
31 the $U_{37}^{K'}$ paleothermometer for two depositional environments (shelf and upper-slope), by
32 means of a Reaction-Transport Model (RTM). RTM results reveal that preferential degradation
33 of $C_{37:3}$ can potentially alter the original signal of the $U_{37}^{K'}$ paleothermometer, but SST biases
34 (Δ SST) are largely within $U_{37}^{K'}$ calibration error (Δ SST < 1.5 °C) assuming realistic model
35 parameters. The magnitude of Δ SST is largely determined by the degradation rate constant, but
36 it also increases with higher differential degradation factors. Additionally, initial $U_{37}^{K'}$ values
37 exert a non-linear influence on the extent of potential SST bias, with mid-range values (0.4
38 < $U_{37}^{K'} < 0.6$) being most sensitive. The most significant changes occur in the shallowest
39 sediment layers and are attenuated with burial time/depth. Scenarios where Δ SST > 1.5 °C are
40 associated with marked downcore decreases in alkenone concentration. Consequently, we
41 caution against the interpretation of $U_{37}^{K'}$ indices when extensive degradation results in very low
42 alkenone concentrations (< 5 ng g⁻¹).

43 *Key-words:* Sea surface temperature; reaction-transport model; paleoceanography;
44 paleoclimate; $U_{37}^{K'}$ paleothermometer, preferential degradation.

45 **1 Introduction**

46 Alkenones are long chain unsaturated ketones (C₃₆-C₃₉; di-, tri-, or tetra-unsaturated) that were
47 first detected in marine sediments by *Boon et al.* [1978] and then systematically identified by
48 *de Leeuw et al.* [1980] and *Volkman et al.* [1980b]. In the present day ocean, the modern
49 biological precursor of these compounds are reticulofenestrated haptophytes, such as *Emiliana*
50 *huxleyi* and *Gephyrocapsa oceanica* [Volkman et al., 1980a, 1980b, 1995; Marlowe et al.,
51 1990; Conte and Eglinton, 1993; Volkman, 2000]. Although the occurrence of alkenones
52 extends to the Cretaceous period [Farrimond et al., 1986; Brassell and Dumitrescu, 2004], the
53 presence of alkenones in Cretaceous sediments is uncommon and restricted to di-unsaturated
54 alkenones, possibly because the C_{37:3} metabolic pathway only developed in response to long-
55 term global cooling [Brassell, 2014]. The oldest observed tri-unsaturated alkenones occur in
56 early Eocene sediments, but even then they are relatively uncommon [Marlowe et al., 1984;
57 Weller and Stein, 2008; Brassell, 2014].

58 Crucially, numerous studies have revealed a relationship between the degree of
59 unsaturation of C₃₇ alkenones (C_{37:2}, C_{37:3}, and C_{37:4}; Figure 1) and algae growth temperature,
60 resulting in the development of the U₃₇^K index as a proxy for sea surface temperature [Brassell
61 et al., 1986]. However, because C_{37:4} alkenone concentrations are typically low (or zero)
62 [Grimalt et al., 2000] and display a high variability in relative abundance and geographic
63 distribution across ocean basins, as well as a poor correlation with SST [Rosell-Melé et al.,
64 1994; Sikes et al., 1997; Sikes and Sicre, 2002; Bendle and Rosell-Melé, 2004], Prahl and
65 Wakeham [1987] and Prahl et al. [1988] proposed the now more widely used U₃₇^{K'} (Eq. 1) index
66 based on the concentrations of C_{37:3} and C_{37:2} alkenones:

$$67 \quad U_{37}^{K'} = \frac{[C_{37:2}]}{[C_{37:2}] + [C_{37:3}]} \quad (\text{Equation 1}).$$

68

69 The quantitative relationship between the $U_{37}^{K'}$ index and ambient growth temperature has been
70 calibrated on the basis of laboratory cultures, as well as on suspended particulate organic matter
71 and sediment coretops [Prahl and Wakeham, 1987; Müller et al., 1998].

72 Alkenones are usually well preserved in the sedimentary record [Sikes et al., 1991;
73 Prahl et al., 2000]. As such, the $U_{37}^{K'}$ paleothermometer is considered diagenetically robust (*i.e.*
74 resistant and/or little altered during diagenesis) and is extensively used to reconstruct past
75 ocean and lake surface temperature [Prahl et al., 2000, 2003; Ho et al., 2013; Brassell, 2014].
76 Consequently, the validity of the proxy relies on the assumptions that alkenones are relatively
77 recalcitrant and, more importantly, that all C_{37} alkenones degrade at similar rates. However,
78 several studies have shown that alkenones can be rapidly degraded in the water column, in
79 marine sediments, and under laboratory conditions [Conte et al., 1992; Freeman and Wakeham,
80 1992; Hoefs et al., 1998; Teece et al., 1998; Gong and Hollander, 1999; Rontani et al., 2005,
81 2008; Rontani and Wakeham, 2008; Huguet et al., 2009]. In addition, unsaturated lipids are
82 generally considered more easily degradable than saturated compounds [Volkman et al., 1983;
83 Cranwell et al., 1987; Grimalt et al., 2000], and different alkenones might thus be degraded at
84 different rates.

85 However, there is conflicting evidence regarding the question whether there is a
86 preferential degradation of $C_{37:3}$ over $C_{37:2}$ alkenones. Several studies found no evidence for
87 preferential degradation [*e.g.*, Prahl et al. 1989, 2000, 2003; Sikes et al. 1991; Conte et al.
88 1992; Rontani et al. 1997; Teece et al. 1998; Grimalt et al. 2000; Herbert, 2001], whereas
89 others directly observed or inferred a higher degradation of the $C_{37:3}$ alkenone [Freeman and
90 Wakeham, 1992; Hoefs et al., 1998; Gong and Hollander, 1999; Rontani et al., 2005, 2008,
91 2013; Huguet et al., 2009]. Their observations indicate that the potential bias in reconstructed
92 SST induced by such a preferential degradation ranges from 0 to up to +5.9 °C under both oxic
93 and anoxic conditions and in both in the water column and sediments [Rontani et al., 2013].

94 Regardless of the main drivers of preferential degradation, a potential diagenetic
95 modification of the primary signal could have important implications for paleoreconstructions
96 and could result in erroneous conclusions. For instance, many Paleogene sediments only
97 contain the C_{37:2} alkenone [*e.g.*, *Marlowe et al.* 1984; *Pagani et al.*, 1999, 2000; *Mercer and*
98 *Zhao*, 2004; *Lyle et al.*, 2006]. These observations could be interpreted as a high SST during
99 the Paleogene or could be the result of preferential degradation of the C_{37:3} alkenone. Much of
100 the scientific debate has revolved around the existence of preferential degradation and its
101 potential controls, whereas little attention has been devoted to quantitatively assessing the
102 potential influence of preferential degradation on the downcore profiles of C_{37:2} and C_{37:3} and
103 thus, the evolution of the U₃₇^{K'} ratio during burial. Such an assessment would not only advance
104 our understanding of the possible impacts of preferential degradation on the U₃₇^{K'} derived
105 paleoreconstructions, but could also help identify the range of conditions (*e.g.* sedimentation
106 rate, concentrations, degradation rate constants) under which preferential degradation could
107 compromise the applicability of the U₃₇^{K'} paleothermometer. Furthermore, it could help
108 disentangle the interplay between preferential degradation and additional processes that can
109 induce SST biases, such as resuspension and lateral transport [*e.g.*, *Benthien and Müller*, 2000;
110 *Ohkouchi et al.*, 2002; *Mollenhauer et al.*, 2003].

111 However, alkenone degradation rate constants are poorly constrained, making it
112 difficult to quantitatively assess the influence of preferential degradation on U₃₇^{K'} derived
113 paleoreconstructions. In addition, extrapolating experimental results of alkenone degradation
114 to geological timescales, especially over a large range of environmental conditions, is not
115 straightforward. Therefore, here we use a reaction-transport model (RTM) approach [*Berner*,
116 1980; *Boudreau*, 1997] to quantitatively assess the potential impact of preferential degradation
117 on the U₃₇^{K'} paleothermometer during burial in marine sediments. The specific aims of this work
118 are to: (1) quantitatively assess the impact of preferential degradation on U₃₇^{K'}

119 paleothermometry; (2) identify the main factors that control SST biases and quantify their
120 relative significance; and (3) based on the model results, evaluate the impact of preferential
121 degradation on the application of the $U_{37}^{K'}$ paleothermometer. With respect to the latter, we
122 revisit previously published data but our goal is not to recalculate published SSTs; rather it is
123 to explore the implications of our sensitivity experiment for such records and provide a guide
124 for critical assessment of the $U_{37}^{K'}$ proxy in future studies.

125

126 **2 Model Description**

127 The RTM approach allows the simultaneous tracking of alkenone concentrations and the
128 sedimentary $U_{37}^{K'}$ indices in a given sediment layer during burial in marine sediments.
129 Additionally, model simulations enable an evaluation and comparison of short- and long-term
130 impacts. Here, we first provide a detailed description of the modelling approach. The model is
131 then used to explore the evolution of the $U_{37}^{K'}$ ratio during burial for different environmental
132 conditions (depositional environments with distinct sediment accumulation rates and
133 bioturbation coefficients), $U_{37}^{K'}$ initial values, and alkenone degradation parameters
134 (degradation rate constant and differential degradation factor between alkenones). We develop
135 a comprehensive sensitivity study that allows us to explore the full range of these parameters,
136 given their poorly constrained nature, in order to establish a quantitative framework for
137 understanding the conditions under which $U_{37}^{K'}$ indices could have been biased. The model
138 developed here is based on the vertically-resolved mass conservation equation for alkenones
139 in marine sediments (Eq. 2) [e.g., Berner, 1980]:

$$140 \quad \frac{\partial C_{37:i}}{\partial t} = - \frac{\partial F_i}{\partial z} + \sum_j R_i^j \text{ (Equation 2),}$$

141 where $C_{37:i}$ is the concentration of alkenone i , z is the sediment depth, t denotes the time, F_i
142 summarizes the advective and dispersive flux divergence of alkenone i and $\sum_j R_i^j$ represents

143 the sum of production/consumption rates j that affect alkenone i . This approach allows the
144 evolution of alkenone concentration to be explored with both burial time and burial depths.
145 Burial depth and time are directly linked via the characteristic timescales of transport processes
146 F_i (*i.e.* in a non-compacting sediment, burial time $t=z/w$). Figure 2 shows a conceptual
147 illustration of the alkenone degradation model applied here and the following sections provide
148 a detailed model description.

149 The model accounts for the advective burial flux of alkenones, as well as the random
150 displacement of sediments caused by the activity of infaunal organisms in the bioturbated zone
151 of the sediment ($z < z_{bio}$), which is described as a dispersive process [Boudreau, 1986] with a
152 constant bioturbation coefficient D_{bio} . The bioturbation coefficient is set to zero below the
153 bioturbated zone. In addition, alkenones are consumed by heterotrophic degradation during
154 burial. The degradation of organic compounds is a multi-step process. However, the initial
155 hydrolysis step is considered to be the rate limiting step and the degradation process is thus
156 generally described as a single step reaction following first order kinetics [*e.g.*, Arnosti, 2011].
157 Traditionally, organic matter reactivity and thus, the reaction rate constant or reactivity, k , of
158 the kinetic rate law is assumed to be controlled by the molecular structure of the organic
159 compound [*e.g.*, Rechka and Maxwell, 1988; Sun and Wakeham, 1994]. In this case, the
160 susceptibility of alkenone $C_{37:i}$ towards microbial degradation would not change during burial
161 and its degradation can thus be described by a constant reactivity k_i . The resulting rate law is
162 equivalent to the so-called 1G Model [*e.g.*, Boudreau 1997]. However, some empirically
163 determined k_i values from pelagic environments and shallow oxic sediments are extremely
164 high. For instance, Gong and Hollander [1999] determined rate constants of $k_i \approx 10^{-3} \text{ yr}^{-1}$ for
165 sediments from the Santa Monica Basin, and Freeman and Wakeham [1992] and Sun and
166 Wakeham [1994] measured a value of $k_i = 9.0 \cdot 10^{-3} \text{ yr}^{-1}$ in sediments from the Black Sea. If
167 applied in a 1G model, such high rate constants would result in a complete alkenone

168 consumption within the upper sediment layer and thus, contradict the observed persistence of
169 alkenones in marine sediments, suggesting that these rate constants are not representative or
170 that alkenone reactivity might decrease with depth/time. Indeed, observations have shown that
171 the reactivity of organic matter is not only controlled by its chemical structure. Organic matter
172 reactivity results from the interplay between the organic matter and its environment, and
173 consequently is not a characteristic attributed solely to organic matter itself [Mayer, 1995].
174 Therefore, the reactivity of the C₃₇ alkenones could, in addition to their molecular structures,
175 also be controlled by factors such as the macromolecular structure in which the compounds are
176 incorporated, oxygen exposure time and terminal electron acceptor availability, microbial
177 community structure, physical protection, and priming [e.g., Aller, 1994; Keil et al., 2004;
178 Burdige, 2006; Zonneveld et al., 2010; Arndt et al., 2013]. In fact, observational evidence
179 indicates that the degradation of lipids, amino acids, carbohydrates, as well as of bulk organic
180 carbon is more similar within a depositional setting than the degradation of individual
181 compounds across sites [e.g., Burdige, 2006]. This suggests that alkenones degrade similarly
182 as bulk organic matter and that additional environmental controls could cause a decrease in
183 apparent alkenone reactivity during burial. Several studies support this hypothesis. They show
184 that additional factors, such as oxygen exposure times [e.g., Gong and Hollander, 1999] and
185 microbial community dynamics [e.g., Rontani et al., 2008], can exert an influence on the
186 apparent reactivity of alkenones, causing k to decrease during burial. Such a decrease in
187 reactivity can be mathematically described by a power law, equivalent to the widely used
188 reactive continuum (RCM) and power models of organic matter degradation [Middelburg,
189 1989; Boudreau and Ruddick, 1991]. Here, we developed two reactivity scenarios to test the
190 influence of preferential degradation on changes in SST assuming (1) a constant alkenone
191 reactivity with burial depth (1G model), based on the classical view of a chemical structure
192 controlled degradation, and (2) a decreasing alkenone reactivity with burial depth (power

193 model/reactive continuum model), based on observational evidence for additional controls on
194 apparent alkenone reactivity.

195

196 *Scenario 1: Constant reactivity, k_i , during burial (1G model) (Eq. 3-4):*

197 Assuming a constant reactivity, k_i , the vertically-resolved mass conservation equation for
198 alkenone concentrations, $C_{37:i}$, in marine sediments can be formulated as:

199
$$\frac{\partial C_{37:i}}{\partial t} = D_{bio} \frac{\partial^2 C_{37:i}}{\partial z^2} + \omega \frac{\partial C_{37:i}}{\partial z} - k_i C_{37:i} \text{ for } z < z_{bio} \text{ (Equation 3)}$$

200
$$\frac{\partial C_{37:i}}{\partial t} = \omega \frac{\partial C_{37:i}}{\partial z} - k_i C_{37:i} \text{ for } z \geq z_{bio} \text{ (Equation 4),}$$

201 where $C_{37:i}$ represents the alkenone ($C_{37:2}$ or $C_{37:3}$) concentration at depth, D_{bio} denotes the
202 bioturbation diffusion coefficient, ω is the burial velocity, and k_i is the first order degradation
203 rate constant for alkenone $C_{37:i}$. A preferential degradation factor $f_{C_{37:3}}$ relates the degradation
204 rate constants k_i of $C_{37:3}$ and $C_{37:2}$ alkenones and thus, serves as a quantitative measure of the
205 extent of preferential degradation:

206
$$k_{37:3} = f_{C_{37:3}} \cdot k_{37:2} \text{ (Equation 5).}$$

207

208

209 *Scenario 2: Decreasing reactivity, $k_i(z)$, during burial (Reactive Continuum Scenario) (Eq. 6-*
210 *7):*

211 A decrease in alkenone reactivity during burial can be mathematically described by a power
212 law and is equivalent to the widely used reactive continuum (RCM) and power models of
213 organic matter degradation [Middelburg, 1989; Boudreau and Ruddick, 1991]. Assuming a
214 decreasing reactivity, $k_i(z)$, the vertically-resolved mass conservation equation for alkenone
215 concentrations, $C_{37:i}$, in marine sediments is then given by:

216
$$\frac{\partial C_{37:i}}{\partial t} = D_{bio} \frac{\partial^2 C_{37:i}}{\partial z^2} + \omega \frac{\partial C_{37:i}}{\partial z} - k_i(z) C_{37:i} \text{ for } z < z_{bio} \text{ (Equation 6)}$$

217
$$\frac{\partial C_{37:i}}{\partial t} = \omega \frac{\partial C_{37:i}}{\partial z} - k_i(z) C_{37:i} \text{ for } z \geq z_{bio} \text{ (Equation 7),}$$

218 where the decrease in $k_i(z)$ with sediment burial age, *burial time*(z), is described in the form of
 219 the power law relationship [Middelburg, 1989; Boudreau and Ruddick, 1991]:

220
$$k_i(z) = \frac{p_i}{a_i + \text{burial time}(z)} \text{ (Equation 8),}$$

221 where p_i and a_i are parameters that determine the depth profile of k_i . The a_i parameter denotes
 222 the apparent initial age of the alkenone mixture in the sediment and can be seen as a shape
 223 parameter, whereas the p_i parameter scales the initial distribution of alkenones [Boudreau and
 224 Ruddick, 1991]. Low a_i and high p_i represent a dominance of more bioavailable alkenones,
 225 whereas high a_i and low p_i represent a dominance of less bioavailable alkenones. Therefore,
 226 the apparent alkenone reactivity in the upper sediment layers will be higher for low a_i values
 227 (more bioavailable alkenones), which results in a rapid loss of alkenones at surface sediments,
 228 but also a rapid decrease in $k_i(z)$ with depth. Alternatively, high a_i values will yield lower
 229 apparent alkenone reactivity close to the sediment-water interface (less bioavailable
 230 alkenones); consequently, alkenones will have lower degradability at surface sediments and
 231 the downcore decrease in $k_i(z)$ will be slower [see Arndt *et al.*, 2013 Fig. 10 for details]. In the
 232 case of the RCM, the preferential degradation factor $f_{C37:3}$ could in theory be applied to both
 233 the a_i and p_i parameter. The parameter p_i merely scales the reactivity of alkenones. The
 234 application of the preferential degradation factor $f_{C37:3}$ to p_i according to

235
$$p_{37:3} = f_{C37:3} \cdot p_{37:2} \text{ (Equation 9)}$$

236 results in a shift of the entire reactivity profile $k_i(z)$ for tri-saturated alkenones to higher
 237 reactivity and is identical to its use in Scenario 1. It is important to note that, in this case, the
 238 1G model represents an end-member RCM scenario, *i.e.* no decrease of alkenone reactivity
 239 with burial time/depth and therefore, can be considered as a ‘worst case’ scenario for a
 240 preferential degradation bias.

241 We can further assume a different decrease in reactivity with burial between the two
242 alkenones. In this case, a preferential degradation arises from a difference in a_i values ($C_{37:3}$
243 more labile than $C_{37:2}$, *i.e.* $a_{37:3} \ll a_{37:2}$) and, thus, the preferential degradation factor would
244 be applied to a_i . Such assumption, however, would suggest that the two alkenones have distinct
245 sources, undergo different transport mechanisms, and/or are differently affected by mineral
246 protection, microbial community dynamics or terminal electron acceptor availability
247 before/during burial. Those assumptions seem unlikely, and if true, would prevent the
248 application of $U_{37}^{K'}$ as a SST proxy. Therefore, we generally assume that the parameter a_i , which
249 controls the shape of the reactivity decrease with depth, is identical for both alkenones.
250 Nonetheless, we also tested this hypothesis to assess the potential SST biases that could arise
251 from such conditions.

252

253 *2.1 Solution*

254 Equations 3-4 and 6-7 can be used to trace the evolution of alkenone concentrations in a given
255 sediment layer during burial by assuming steady state conditions ($\frac{\partial C}{\partial t} = 0$) and a constant
256 porosity, thus neglecting sediment compaction. In addition, we also assume that benthic
257 activity efficiently mixes material in the bioturbated layer, resulting in a constant age. Burial
258 time (*i.e.* the age of a given sediment layer) and burial depth, z , are then related by:

259

260 $burial\ time(z) = 0$ for $z < z_{bio}$ (Equation 10),

261 $burial\ time(z) = \frac{z - z_{bio}}{\omega}$ for $z \geq z_{bio}$ (Equation 11).

262 The integration of Eqs. 3-4 and 6-7 can then be solved analytically and yield the following
263 general solutions representing the evolution of alkenone concentrations with burial depth/time:

264

265 *Scenario 1: Constant reactivity, k_i , during burial (1G Scenario) (Eq. 3-4):*

266
$$C_{37:i}(z) = A_1 e^{a_1 \cdot z} + B_1 e^{b_1 \cdot z} \text{ for } z < z_{bio} \text{ (Equation 12)}$$

267
$$C_{37:i}(z) = A_2 e^{a_2 \cdot z} \text{ for } z \geq z_{bio} \text{ (Equation 13)}$$

268 where:

269
$$a_1 = \frac{\omega - \sqrt{\omega^2 + 4 \cdot D_{bio} \cdot k_i}}{2 \cdot D_{bio}} \text{ (Equation 14)}$$

270
$$b_1 = \frac{\omega + \sqrt{\omega^2 + 4 \cdot D_{bio} \cdot k_i}}{2 \cdot D_{bio}} \text{ (Equation 15)}$$

271
$$a_2 = \frac{-k_i}{\omega} \text{ (Equation 16)}$$

272 Determining the integration constants A1, B1 and A2 requires the definition of boundary
273 conditions. Here, we assume:

274

275 (1) a known concentration of the alkenones at the sediment water interface

276
$$C_{37:i}(0) = C_{37:i,0} \text{ (Equation 17);}$$

277 and (2 and 3) continuity between the bioturbated and non-bioturbated zone:

278
$$(2) C_{37:i,1}(z_{bio}) = C_{37:i,2}(z_{bio}) \text{ (Equation 18);}$$

279
$$(3) D_{bio} \cdot \frac{\partial C_{z_{bio}}}{\partial z} |_{z_{bio}} = 0 \text{ (Equation 19).}$$

280

281 *Scenario 2: Decreasing reactivity, $k_i(z)$, during burial (Eq. 5-6; RCM Scenario):*

282
$$C_{37:i}(z) = A_1 e^{a_1 \cdot z} + B_1 e^{b_1 \cdot z} \text{ for } z < z_{bio} \text{ (Equation 20)}$$

283
$$C_{37:i}(z) = C_{37:i}(z_{bio}) \cdot \left(\frac{a_i}{a_i + \text{burial time}(z)} \right)^{-p_i} \text{ for } z \geq z_{bio} \text{ (Equation 21)}$$

284 where:

285
$$a_1 = \frac{\omega - \sqrt{\omega^2 + 4 \cdot D_{bio} \cdot p_i / a_i}}{2 \cdot D_{bio}} \text{ (Equation 22)}$$

286
$$b_1 = \frac{\omega + \sqrt{\omega^2 + 4 \cdot D_{bio} \cdot p_i/a_i}}{2 \cdot D_{bio}} \text{ (Equation 23)}$$

287 Eq. 6 is thus mathematically equivalent to Eq. 3 with reactivity $k_i(z) = p_i/a_i$ (Equation 24),
288 within the bioturbated layer.

289 Determining the integration constants A1, B1 requires the definition of boundary conditions.
290 Here, we assume:

291 (1) a known alkenone concentration at the sediment water interface

292
$$C_{37:i}(0) = C_{37:i,0} \text{ (Equation 25);}$$

293 (2) continuity between the bioturbated and non-bioturbated zone:

294
$$(2) D_{bio} \cdot \frac{\partial C_{z_{bio}}}{\partial z} |_{z_{bio}} = 0 \text{ (Equation 26).}$$

295

296 *2.2 Model Parameters and Boundary Conditions*

297 Model parameters and boundary conditions place the model in its environmental context. Table
298 1 provides an overview of the respective model parameters and boundary conditions, their units
299 and their values. Model parameters can be divided into those that define the general
300 depositional environment and are generally well constrained, and those that control alkenone
301 degradation and are generally variable and/or poorly constrained. Therefore, a two-step
302 sensitivity study is conducted here. Model simulations are carried out for two different
303 depositional environments (coastal sediments – water depth 200 meters; and upper slope
304 sediments – water depth 1000 meters) to explore their potential impact on preferential
305 degradation and the $U_{37}^{K'}$ paleothermometer. In addition, for each depositional setting, a
306 sensitivity study is conducted over the entire range of plausible degradation parameters to
307 account for the parameter uncertainty of degradation parameters.

308

309

310 2.2.1 Sensitivity to Depositional Environment

311 In marine sediments, burial depth and time are directly linked via the characteristic timescales
312 of transport processes (Eq. 10-11) and, thus, the bioturbation coefficient, bioturbation depth
313 and burial velocity. The model calculates the alkenone concentration depth profiles for both a
314 typical coastal sediment, as well as an upper slope sediment up to a maximum sediment column
315 depth of 250 meters.

316 Based on a compilation of mixing layer depths [*Boudreau*, 1994, 1998], the depth of
317 the bioturbated zone is set to 10 cm for both water depth scenarios. Bioturbation coefficients
318 and burial velocities are determined based on a water depth dependent relationship proposed
319 by *Middelburg et al.* [1997]. This approach aims at providing a general framework for potential
320 alkenone bias with burial time/depth for contrasting depositional environments rather than
321 simulating any specific setting. Note that, since the model traces the evolution of alkenone
322 layers during burial, (likely) changes in sedimentation rate over burial time would merely have
323 an impact on the calculation of burial depth (Eq. 11). For instance, a decrease in sedimentation
324 rate would simply reduce burial depth for a given burial time, but would not have an impact on
325 the simulated SST bias and, thus, the overall results. Although C₃₇ alkenone concentrations at
326 the sediment water interface (SWI) can be highly variable depending on local primary
327 production rates and vertical transport in the water column, sediment trap and surface sediment
328 studies [*Gong and Hollander*, 1999; *Müller and Fischer*, 2001; *Prahl et al.*, 2001; *Rodrigo-*
329 *Gámiz et al.*, 2016] indicate that alkenone concentrations in settling suspended matter and
330 surface sediments typically range from approx. 4 – 77 µg g⁻¹. Thus, the total C₃₇ alkenone
331 (C_{37:2} + C_{37:3}) concentration at the SWI was set to 5 µg g⁻¹.

332

333

334

335 2.2.2 Sensitivity to Uncertainty in Degradation Rate Parameters

336 Most of the parameters that control the potential degree of preferential degradation (such as the
337 initial $U_{37}^{K'}$ of the material that has been deposited at SWI, $U_{37}^{K'}(0)$; the degradation rate
338 constant, k_i ; and the differential degradation factor between di- and tri-unsaturated C₃₇
339 alkenones, $f_{C37:3}$) are either variable and/or difficult to constrain. Therefore, we designed a
340 comprehensive parameter sensitivity study in order to assess the response of alkenone
341 concentration depth profiles and thus, the $U_{37}^{K'}$ ratio to different degrees of preferential
342 degradation. The evolution of alkenone concentrations with burial time/depth is thus simulated
343 over the entire plausible parameter range of: i) the initial $U_{37}^{K'}$, $U_{37}^{K'}(0)$; ii) the degradation rate
344 constant, k_i ; and iii) the differential degradation factor between di- and tri-unsaturated C₃₇
345 alkenones, $f_{C37:3}$.

346 The $U_{37}^{K'}(0)$ was varied over the entire range of 0.1 to 0.9 $U_{37}^{K'}$ units only excluding $U_{37}^{K'}$
347 = 0 and $U_{37}^{K'} = 1$, reflecting the absence of C_{37:2} and C_{37:3}, respectively. Degradation rate
348 constants, k_i , are notoriously difficult to constrain. First order rate constants derived from
349 laboratory experiments [Teece *et al.*, 1998] are often not directly transferable to marine
350 sediments characterized by low or no oxygen exposure, low temperature and high pressure
351 [Schouten *et al.*, 2010] and estimates from the field are highly variable [*e.g.*, Sun and Wakeham,
352 1994; Gong and Hollander, 1999]. Therefore, we do not rely on these rate constant values;
353 instead, we explore the entire range of potential values. However, we do interpret the model
354 results in the context of these experimental and field estimates (see *Section 4.1*). Model-derived
355 first-order degradation rate constants of bulk organic matter typically vary by several orders of
356 magnitude, from as high as 10^1 yr^{-1} to as low as 10^{-9} yr^{-1} [Arndt *et al.*, 2013]. Therefore, we
357 vary the first order degradation rate constant k_i from 10^{-5} to 10^{-3} yr^{-1} (1G model). The lower
358 limit is set to 10^{-5} yr^{-1} , because lower degradation rate constants result in a negligible effect of
359 preferential degradation on $U_{37}^{K'}$; as such, this study represents a ‘worst case scenario’ for $U_{37}^{K'}$

360 bias. The upper limit is defined as 10^{-3} yr^{-1} , because levels higher than that seem unrealistic,
361 since they result in complete consumption of alkenones in the sediment surface layer.

362 Similar to constant first order degradation rate constants, the free parameters p and a
363 that control the shape of the $k_i(z)$ depth profile are also difficult to constrain. Model-derived
364 parameters from a wide range of different environments indicate that p generally falls within
365 the range between 10^{-2} and 10^0 , while the parameter a may vary over several orders of
366 magnitude from 10^{-1} to 10^6 yrs [Arndt *et al.*, 2013]. Here, the free parameter a_i varies from 10^{-1}
367 to 10^4 yrs, whereas p_i varies from 10^{-2} to 10^0 . We, therefore, explore the entire range of
368 plausible degradation rate constants for both the 1G model and the RCM scenario.

369 To simulate the preferential degradation of tri-unsaturated alkenones, a ratio between
370 the $C_{37:3}$ degradation rate constant and the $C_{37:2}$ degradation rate constant – a preferential
371 degradation factor $f_{C_{37:3}}$ – is defined and varied from 1.1 to 1.5 (*i.e.* $C_{37:3}$ degradation is 10%
372 to 50% faster than the degradation of $C_{37:2}$). This range has been informed by observed
373 differences of preferential alkenones degradation in field and laboratory experiments [*e.g.*,
374 Hoefs *et al.*, 1998; Gong and Hollander, 1999; Rontani *et al.*, 2005, 2008].

375

376 2.3 Model Output

377 The model calculates the evolution of individual alkenone concentrations over burial
378 time/depth (Eq. 3-4 and 6-7). Based on these simulated concentrations, $U_{37}^{K'}$ ratios are calculated
379 according to Eq. 1. SSTs are estimated based on the calculated $U_{37}^{K'}$ ratios using the global core-
380 top calibration of Müller *et al.* [1998] (Table 1). SST is calculated from the SWI down to 250
381 meter below sea floor (mbsf) for the parameter combinations described in Table 1. The
382 deviation of the estimated SST from the original SST recorded by the material deposited at the
383 sediment-water interface or, in other words, the SST bias due to preferential degradation
384 (Δ SST; Table 1) is calculated for typical burial depths 50, 100, 150, 200, and 250 mbsf. For

385 the hypothetical coastal sediments (200 meters depth), those depths represent burial times of
386 approximately 14 kyr, 28 kyr, 42 kyr, 55 kyr, and 70 kyr, respectively. For the hypothetical
387 upper slope sediments (1000 meters depth), those depths correspond to 31 kyr, 62 kyr, 94 kyr,
388 125 kyr, and 156 kyr, respectively.

389

390 **3 Results**

391 In the following sections, we mainly focus on the findings derived from the 1G approach
392 (Figures 3 – 6; Table 2) or, in other words, the ‘worst case’ endmember RCM scenario
393 (negligible decrease in k_i with depth/time) described in Section 2.2. We do so because that
394 approach results in the most extensive degradation and, thus, SST bias. As such, simulation
395 results will help to delineate a conservative range of conditions that favor preferential
396 degradation and potentially result in SST bias. The discussion of the 1G – ‘worst case’ RCM –
397 simulation results are supplemented with simulation results from Scenario 2 (Figures 7 – 10),
398 in which we test a broad range of a_i and p_i values.

399 Figures 3 to 6 summarize changes in the $U_{37}^{K'}$ derived SSTs and alkenone concentrations
400 as a function of all parameters explored in the Scenario 1. To illustrate the effect of preferential
401 degradation on Δ SST (*i.e.* the deviation from the real SST) for a wide range of degradation
402 scenarios and environmental conditions, interpolated plots of simulated Δ SST over the
403 simulated $U_{37}^{K'}$ (0) and $f_{C37:3}$ space are produced for each water depth (Fig. 3-6 a and b, two
404 columns: 200 m and 1000 m), different burial depths/times (Fig. 3-6 a and b, 5 panels per
405 column: 50 mbsf, 100 mbsf, 150 mbsf, 200 mbsf and 250 mbsf), and degradation rate constants
406 (Fig. 3-6). The simulated burial depths represent sediment ages ranging from 14 kyr to 70 kyr
407 and from 31 kyr to 156 kyr for the shallow and deep site, respectively. In addition, vertical
408 profiles of the preserved fraction of the original deposited total alkenone ($C_{37:2}+C_{37:3}$)
409 concentration over burial depth/time are plotted to visualize the decrease in total alkenone

410 concentrations (Fig. 3-6 c and d). Furthermore, Table 2 summarizes the range of Δ SST values
411 and C_{37} alkenone extent of degradation throughout all scenarios explored in Scenario 1.

412 The 1G simulations (Fig. 3-6) show that the impact of preferential degradation on $U_{37}^{K'}$
413 ratios and, thus, the positive bias in reconstructed SST ranges from less than 0.1 °C in the least
414 reactive and/or least selective degradation scenario ($k_{37:2} = 1.0 \cdot 10^{-5} \text{ yr}^{-1}$; $f_{C37:3} = 1.1$; $U_{37}^{K'}(0) =$
415 0.1 and 0.9) up to 27 °C in the most extreme ($k_{37:2} > 1.0 \cdot 10^{-4} \text{ yr}^{-1}$; $f_{C37:3} > 1.4$; $U_{37}^{K'}(0) = 0.1$),
416 albeit unrealistic (see below), scenario (Table 2; Figures 3 to 6). In general, the influence of
417 preferential degradation on the bias in reconstructed SST is controlled by a combination of
418 factors. The most important factors are the degradation rate constants k_i , the initial $U_{37}^{K'}(0)$
419 value and the preferential degradation factor $f_{C37:3}$, while water depth (and thus, the general
420 depositional environment) exerts an important but subordinate impact. In addition, the lower
421 panels c and d (Fig. 3-6) illustrate the dramatic influence of increasing degradation rate
422 constants, k_i , on alkenone concentrations and their downcore preservation. For example, when
423 k_i is assumed to be $1.0 \cdot 10^{-4} \text{ yr}^{-1}$, then less than 1% of the originally deposited alkenones are
424 preserved at a burial depth of 50 mbsf.

425 In general, Δ SST increases with an increase in alkenone degradation rate constants, k_i ,
426 and preferential degradation factor, $f_{C37:3}$. An extremely high k_i ($1.0 \cdot 10^{-3} \text{ year}^{-1}$) yields a large
427 Δ SST ($\sim 27 \text{ °C}$) and extensive loss of C_{37} alkenone ($\gg 99.9\%$, results not shown). Yet, such
428 an extreme distortion of the $U_{37}^{K'}$ seems unlikely, given the fact that alkenones are generally
429 well preserved, even in highly oxidising sediments [*e.g.*, *Prahl et al.*, 1989, 2003]. Lower k_i
430 values ($k_i < 2.5 \cdot 10^{-5} \text{ year}^{-1}$) result in lower alkenone degradation rates (fraction degraded at
431 250 mbsf is $< 99\%$) and, thus, represent more plausible scenarios. In addition, Fig. 3-6 show
432 that maximum Δ SST is generally observed for mid-range $U_{37}^{K'}(0)$, and Δ SST is smaller when
433 initial $U_{37}^{K'}(0)$ values are low or high (Fig. 3). This is especially true for high indices ($U_{37}^{K'}(0) >$
434 0.8), which, of course, have a limited capacity to increase further. Even low initial $U_{37}^{K'}(0)$

435 values are relatively robust under low degradation scenarios (Fig. 3). However, an increase in
436 alkenone degradation, due to higher degradation rate constants (Fig. 5-6) and/or water and
437 burial depths (a-b), shifts the Δ SST maximum from mid $U_{37}^{K'}(0)$ values towards lower $U_{37}^{K'}(0)$
438 values ($U_{37}^{K'}(0) < 0.2$) (Figure 6).

439 Similar to Scenario 1 (constant reactivity, k_i), Scenario 2 simulations (RCM approach,
440 decreasing reactivity with burial time/depth, $k_i(z)$) can be assessed in the context of all
441 parameters summarized in Table 1. Figures 7 and 8 illustrate changes in the $U_{37}^{K'}$ derived SSTs
442 and alkenone concentrations for each depositional environment and assuming $a_i = 10^0$ yr and
443 $a_i = 10^3$ yr, respectively, and $p_i = 10^{-1}$ (see above for figure details).

444 As already pointed out in section 2, a decrease in degradation rate constant k_i results in
445 generally lower SST biases over the considered burial times. For higher initial alkenone
446 reactivity ($a_i = 10^0$ yr), Δ SST does not exceed 6 °C (Figure 7), and Δ SST < 2 °C for less reactive,
447 but slowly decreasing alkenone reactivity ($a_i = 10^3$ yr; Figure 8). Similar to Scenario 1, SST
448 bias increases with an increase in preferential degradation factor ($f_{C37:3}$), and the maximum
449 Δ SST is generally observed for the mid-range $U_{37}^{K'}(0)$ values and decreases when $U_{37}^{K'}(0)$
450 values are either low or high. Unlike Scenario 1 (constant reactivity), the most significant
451 changes occur in the upper sediment layers and Δ SST, as well as the degree of loss of alkenones
452 (Figure 7-8, c-d) becomes attenuated with burial time/depth, due to the decrease in reactivity
453 ($k_i(z)$). Figure 9 illustrates the decrease in $k_i(z)$ with burial time/depth, assuming $p_i = 10^{-1}$ for a_i
454 = 10^0 yr (Figure 9a) and $a_i = 10^3$ yr (Figure 9b). The lower a_i value results in a higher reactivity
455 ($k_i(0) \approx 10^{-1}$ yr⁻¹) close to the sediment-water interface. However, $k_i(z)$ decreases quickly in the
456 upper sediment layers to $k_i(z) < 10^{-5}$ yr⁻¹ at 50 mbsf and only decreases very slowly with
457 increasing burial time/depth. The higher a_i value results in a lower reactivity ($k_i(0) \approx 10^{-4}$ yr⁻¹)
458 close to the sediment-water interface, but decreases very slowly with burial time/depth.
459 However, at greater burial depth, where burial time $t \gg a_i$, alkenone reactivity approaches

460 similar values as for lower a_i values ($k_i(z) < 10^{-5} \text{ yr}^{-1}$) because Eq. 8 becomes dominated by
461 burial time instead of a_i . Thus, even with distinct $k_i(0)$, increasing burial time/depth yields
462 similar $k_i(z)$ -values and these change much slowly than those of upper sediment layers. The
463 rapid decrease in $k_i(z)$ means that the degradation induced bias in SST is small and generally
464 does not exceed the $U_{37}^{K'}$ calibration error. In detail, high a_i values (Fig. 9b) reflect an overall
465 low reactivity and yield a slow downcore decrease in $k_i(z)$, resulting in minor changes in SST
466 (Fig. 8). The largest ΔSST ($\sim 6 \text{ }^\circ\text{C}$) are generally associated with low a_i value ($a_i = 10^{-1} \text{ yr}$) and
467 high preferential degradation factors $f_{C_{37:3}} = 1.5$ (Fig. 7). Such low a_i values produce the most
468 dramatic decrease in $k_i(z)$ with depth (Fig. 9a) and, thus, represent the most heterogeneous
469 distribution of alkenone reactivity.

470 Although unlikely, we can also explore the impact of differential evolution of alkenone
471 reactivity with burial time, *i.e.* assuming different a_i values for the di- and tri-unsaturated
472 alkenone pools ($C_{37:3}$ more labile than $C_{37:2}$). Figure 10 presents the simulated evolution of $k_i(z)$
473 and SST with burial time/depth, assuming an initially high but rapidly decreasing reactivity for
474 the $C_{37:3}$ pool ($a_{C_{37:3}} = 0.1 \text{ yr}$) and an initially low but slowly decreasing reactivity for the $C_{37:2}$
475 pool ($a_{C_{37:2}} = 100 \text{ yrs}$). This represents an extreme case scenario, since it assumes a large
476 difference in the evolution of the reactivity with burial depth/time (Fig. 10a). The degradation
477 rate constant $k_{C_{37:3}}$ is three order of magnitude higher than $k_{C_{37:2}}$ in the surface sediments. The
478 rate constants then decrease at different rates with burial depth, before reaching similar
479 magnitudes in deeper sediment layers ($> 50 \text{ mbsf}$). Fig. 10b shows that the largest SST changes
480 occur in the shallowest sediment layers, with the most pronounced ΔSST ($> 10 \text{ }^\circ\text{C}$) for $U_{37}^{K'}(0)$
481 < 0.5 . Deeper in the sediment, degradation rates and SST biases significantly slow down.

482 Overall, the decrease in $k_i(z)$ with burial time/depth (Scenario 2) could explain the
483 discrepancy between the fast degradation rates observed in laboratory experiments [Teece *et*
484 *al.*, 1998; Rontani *et al.*, 2005, 2008], as well as field observations [Sun and Wakeham, 1994;

485 *Gong and Hollander, 1999*] and the long-term persistence of alkenones in the geological record
486 [*Brassell, 2014*]. In addition, simulation results indicate that Scenario 2 (decrease in $k_i(z)$ with
487 burial time/depth) generally results in limited SST biases often below the detection limit. In
488 contrast, Scenario 1 (constant k_i) results in more pronounced SST bias and thus, serves as ‘worst
489 case’ endmember scenario and provides a conservative framework to further investigate SST
490 bias. The following sections assess the role of different controls on preferential alkenone
491 degradation in altering $U_{37}^{K'}$ during burial and thus, inducing biases in reconstructed SSTs.

492

493 **4 Discussion**

494 *4.1 Disentangling the controls on SST bias during burial*

495 Overall, both 1G (Scenario 1) and RCM (Scenario 2) simulations indicate that the following
496 three factors control the magnitude of diagenetic modification on $U_{37}^{K'}$ indices: 1) the extent of
497 alkenone degradation, which, in turn, is controlled by the degradation rate constant, k_i , the
498 burial depth, z , and the water depth; 2) the initial $U_{37}^{K'}$ value, $U_{37}^{K'}(0)$; and 3) the preferential
499 degradation factor, $f_{C37:3}$. It is important to note that the influence of these three factors on
500 Δ SST is tightly linked. For instance, the extent of degradation exerts no impact on Δ SST if
501 there is no preferential degradation and vice versa. We also note that our simulations include
502 scenarios in which intense alkenone degradation results in concentrations below the detection
503 limit ($< 5 \text{ ng g}^{-1}$), *i.e.* situations where $U_{37}^{K'}$ could not be determined. Therefore, for the
504 remainder of the discussion we only consider model results in which $> 0.1\%$ of the original
505 alkenone concentration is preserved.

506

507

508

509

510 4.1.1 Extent of degradation

511 Scenarios 1 and 2 reveal that the extent of degradation – as a cumulative effect of k_i , as well as
512 water and burial depths/time – is the major control on Δ SST. The positive bias in U_{37}^{Kl} generally
513 increases with an increasing extent of degradation during burial (Fig. 3-8).

514 The alkenone degradation rate constant, k_i , exerts an important control on the extent of
515 degradation. The reconstructed Δ SST increases from < 0.1 °C to up to 27 °C with an increase
516 in degradation rate from $1.0 \cdot 10^{-5}$ yr⁻¹ to $1.0 \cdot 10^{-4}$ yr⁻¹ (Fig. 3-6). This is particularly critical as
517 alkenone degradation rate constants are difficult to constrain and also implicitly account for
518 factors that control alkenone degradation during burial, but are not explicitly accounted for in
519 the model [Arndt *et al.*, 2013]. Of all k_i values assessed in the present RTM study, $k_i < 1.0 \cdot 10^{-5}$
520 yr⁻¹ seems to best represent the reactivity of alkenones in the sedimentary archive. This refers
521 not only to SST biases (Δ SST < 6.0 °C), but also to the amounts of alkenones degraded. The
522 adoption of faster, and constant, k_i (e.g. $k_i > 5.0 \cdot 10^{-5}$ year⁻¹) results in an almost complete
523 degradation of alkenones ($\gg 99.9\%$), which is inconsistent with their apparent persistence in
524 the sedimentary record [Brassell, 2014]. However, experimentally derived k_i values obtained
525 by Teece *et al.* [1998] for C_{37:3} are four orders of magnitude higher than what we infer to be
526 our most realistic values, if those values are assumed to be constant with burial time/depth.
527 Similarly, Rontani *et al.* [2005, 2008] also report k_i values in the order of 10⁻¹ yr⁻¹ for alkenones
528 in degradation laboratory experiments. However, these rate constants were derived from fresh
529 alkenone material in laboratory incubations, where conditions were optimized to investigate
530 alkenone degradation. This experimental setting could result in a ‘priming effect’ and enhance
531 the degradation of more recalcitrant material [Aller, 1994; Aller and Blair, 2006]. Therefore,
532 they do not account for the complexity of natural conditions [Schouten *et al.*, 2010], and it
533 seems likely that these experiments represent unrealistically high degradation rates compared
534 to natural settings. Environmental conditions that likely account for the lower degradation rates

535 include changes in terminal electrons availability (TEA) (e.g. O₂ availability) and/or packing
536 in macromolecular complexes or mineral particles, which would slow down or prevent
537 microbial attack [see *Arndt et al.*, 2013 and references therein for overview].

538 The extent of alkenone degradation in sediments also depends on water and burial
539 depths/times and thus, the physical depositional environment, which exerts a positive, albeit
540 secondary control. Alkenones deposited in deeper waters experience a greater degree of
541 degradation at similar burial depths, due to slower burial rates or in other words longer burial
542 times [*Middelburg et al.*, 1997]. This effect is consistent with observational data. *Conte et al.*
543 [1992] observed a rapid and significant (by 1-2 orders of magnitude) degradation of alkenones
544 in deep North Pacific waters. In particular, burial depth and, thus, burial time controls the extent
545 of degradation. Longer burial time (*i.e.* deeper depths in the sediment) allows for a longer
546 exposure of alkenones to heterotrophic degradation, therefore resulting in more intensive
547 degradation and ultimately a stronger bias in SST. This becomes evident in Fig 3-6 (Scenario
548 1). Assuming the least dramatic condition (Fig. 3), the maximum perturbation in SST increases
549 from < 2 °C at 50 mbsf to up to 6 °C at 250 mbsf. Alternatively, scenarios with higher k_i values
550 (Fig. 6), yield Δ SST of 10 °C at 50 mbsf and 27 °C at 250 m. Although unrealistic, the latter
551 illustrates how burial depth, as a component of extent of degradation, controls SST biases.
552 However, in Scenario 2, burial time/depth becomes less important with time/depth (Fig. 7-8),
553 due to the decrease of $k_i(z)$ (Fig. 9). In fact, under such conditions, $k_i(z)$ and SST bias become
554 attenuated at greater depths.

555

556 4.1.2 The initial $U_{37}^{K'}$ value

557 Initial $U_{37}^{K'}$ values at the SWI ($U_{37}^{K'}(0)$) exert a non-linear effect on Δ SST during burial and mid-
558 range values ($U_{37}^{K'} \approx 0.5$) generally exhibit the most pronounced SST bias (Fig. 3-4 and 7-8).
559 As *Hoefs et al.* [1998] previously pointed out, such a result is mathematically expected and is

560 the likely explanation for the disagreement between experimental alkenone degradation
561 studies. Under similar conditions, *Rontani et al.* [1997] and *Teece et al.* [1998] found no
562 significant degradation-induced changes in $U_{37}^{K'}$, whereas *Rontani et al.* [2005] later observed
563 a positive degradation-induced bias of 0.1 $U_{37}^{K'}$ units. *Rontani et al.* [2005] argued that the
564 different outcome of these degradation experiments can be explained by different initial $U_{37}^{K'}$
565 values: 0.49 in *Rontani et al.* [2005]; 0.75 in *Teece et al.* [1998]; and 0.85 in *Rontani et al.*
566 [1997]. Model results confirm that $U_{37}^{K'}$ values are relatively robust towards preferential
567 degradation for both high and low $U_{37}^{K'}(0)$ when the extent of degradation is low (low k_i ,
568 shallow sediment depth/short burial times; Fig. 3-4 and 7-8). However, low $U_{37}^{K'}(0)$ initial
569 conditions become more sensitive to diagenetic alteration under intense degradation scenarios
570 (high k_i , low sedimentation rate, deep burial depth/ long burial times), and maximum Δ SST
571 shifts to low $U_{37}^{K'}(0)$ under such conditions (Fig 5-6).

572 The combined effects of degradation extent and $U_{37}^{K'}(0)$ are illustrated in Fig. 11. This
573 shows how the extent of degradation exerts a first order control on Δ SST, with $U_{37}^{K'}(0)$ exerting
574 a lesser and non-linear SST bias. Moreover, $U_{37}^{K'}(0) = 0.5$ is most prone to SST biases when
575 degradation is low and lower values of $U_{37}^{K'}(0)$ are more prone to SST biases when degradation
576 is extensive.

577

578 4.1.3 Preferential degradation factor

579 The preferential degradation factor $f_{C_{37:3}}$ is the parameter that ultimately controls the difference
580 between the degradation rates of the di- and tri-unsaturated C_{37} alkenones. Regardless of the
581 environmental triggers for C_{37} selective degradation (see Introduction), RTM results show that
582 an increase in $f_{C_{37:3}}$ and thus, a more pronounced preferential degradation of $C_{37:3}$ generally
583 leads to a pronounced increase in Δ SST (Figure 3-8). However, the sensitivity of $U_{37}^{K'}$ and Δ SST

584 to an increase in $f_{C37:3}$ depends on the extent of degradation and thus, the degradation rate
585 constant k_i . Even high $f_{C37:3}$ values of 1.5 only induce small Δ SSTs unless the degradation rate
586 constant is large.

587 Additionally, the impact of $f_{C37:3}$ on Δ SST is also dependent on the $U_{37}^{K'}(0)$. As
588 previously pointed out, Δ SST is mostly affected when $U_{37}^{K'}(0) = 0.5$ and the extent of
589 degradation is low. Thus, the preferential degradation factor $f_{C37:3}$ most impacts mid-range
590 values of $U_{37}^{K'}(0)$. Figure 12, assuming a constant degradation rate (*e.g.* $k_i = 5 \cdot 10^{-5} \text{ yr}^{-1}$), allows
591 us to explore the effects of $f_{C37:3}$ and $U_{37}^{K'}(0)$ on Δ SST. For the lowest $f_{C37:3} = 1.1$ (Fig. 12a),
592 the change in SST shows a linear downcore trend; the $U_{37}^{K'}(0) = 0.5$ yields the largest SST
593 perturbation, whereas the high-end $U_{37}^{K'}(0)$ value is the least altered. Increasing the preferential
594 degradation factor to $f_{C37:3} = 1.2$ (Fig. 12b) and $f_{C37:3} = 1.3$ (Fig. 12c) results in a non-linear
595 Δ SST, as well as a shift towards maximum Δ SST occurring at lower $U_{37}^{K'}(0)$ values. These
596 results arise because increasing $f_{C37:3}$ values results in preferential loss of $C_{37:3}$ alkenone and
597 therefore, stronger biases at the lower-end of $U_{37}^{K'}(0)$. Overall and as expected, it is clear that
598 $f_{C37:3}$ exerts a direct control on SST biases. However, only high $f_{C37:3}$ values in combination
599 with intense degradation rates (*i.e.* high k_i) induce Δ SST larger than the $U_{37}^{K'}$ calibration error.
600 Model results emphasize the need to better constrain $f_{C37:3}$ values in natural settings and to
601 identify the factors that control the preferential degradation of $C_{37:3}$. Laboratory incubation
602 experiments performed by Teece *et al.* [1998] found negligible differences in $C_{37:2}$ and $C_{37:3}$
603 alkenone degradation rates, yielding $f_{C37:3} \approx 1.0$. Later experiments conducted by Rontani *et al.*
604 [2008] were able to produce up to 3 °C positive SST biases; given that $U_{37}^{K'}(0) > 0.7$ in that
605 study, a 3 °C Δ SST yields $f_{C37:3} \sim 1.2$. Similar analyses can be conducted for field studies (Table
606 3) and explain apparently contradictory behavior. For example, at the Peruvian Margin,
607 McCaffrey *et al.* [1990] found an alkenone loss of 30% in the top 1 cm of sediments underlying

608 anoxic waters, but $U_{37}^{K'}$ was largely unaffected. Our model results show that when $f_{C37:3} < 1.5$,
609 the extent of degradation must exceed 50% to yield measurable Δ SST. *Prahl et al.* [1989,
610 2003] observed extensive loss of alkenones in the Madeira Abyssal Plain (MAP) turbidites (86
611 – 99%), but only minor changes in $U_{37}^{K'}$ indices (Δ SST < 1.3 °C for $U_{37}^{K'}(0) \geq 0.7$). Model results
612 indicate that this requires a preferential degradation factor $f_{C37:3}$ between 1.1 and 1.2 for the
613 MAP turbidites. *Hoefs et al.* [1998] reported a $> 99\%$ extent of degradation associated with a
614 +0.17 increase in $U_{37}^{K'}$ indices (*i.e.* Δ SST ~ 5 °C), which yields an $f_{C37:3} \sim 1.3$ in our simulations.
615 There is also evidence that $f_{C37:3}$ differs between oxic and anoxic settings. In the Santa Monica
616 Basin sediments, *Gong and Hollander* [1999] compared $U_{37}^{K'}$ records from two adjacent areas
617 and observed a difference in reconstructed SST of up to 4 °C, with oxic settings recording
618 higher temperatures than anoxic ones. However, the extent of degradation was 60% for both
619 settings, indicating that $f_{C37:3}$ differed between the two, being ~ 1.3 and ~ 1.0 in the oxic and
620 anoxic settings (assuming no preferential degradation at the anoxic setting), respectively.

621 Preferential degradation under aerobic conditions [*Hoefs et al.*, 1998; *Gong and*
622 *Hollander*, 1999] has been attributed to preferential degradation of the tri-unsaturated $C_{37:3}$
623 alkenone via double bond epoxidation [*Rontani et al.*, 2008]. This process occurs more
624 effectively at position $\omega 29$, only present on the $C_{37:3}$ alkenone, rather than positions $\omega 15$ and
625 $\omega 22$ which occur on both C_{37} alkenones, and is suggested to be mediated by the bacterial strain
626 *Dietzia maris* sp. S1 [*Rontani and Wakeham*, 2008; *Zabeti et al.*, 2010]. Despite this, it appears
627 that aerobic microbially-mediated selective degradation occurs in a non-systematic way
628 [*Rontani et al.*, 2005, 2008; *Rontani and Wakeham*, 2008], which compromises our ability to
629 quantify and predict its controls on preferential degradation in marine sediments. Moreover, as
630 discussed above, $f_{C37:3}$ appears to be consistently greater than 1 in a variety of settings such that
631 it cannot be solely dependent on oxic/anoxic conditions [*Rontani and Wakeham*, 2008].

632

633 4.2 Implications for $U_{37}^{K'}$ paleothermometry

634 Our model exploration of alkenone degradation provides a quantitative framework for
635 assessing SST reconstructions. Here, we illustrate how model results can be used to explore or
636 offer alternative explanations for SST mismatches in the sedimentary archive.

637 First, the magnitude of SST bias will depend on the initial $U_{37}^{K'}$ value. As previously
638 discussed (Section 4.1.2), high $U_{37}^{K'}$ values are least affected, implying that the alkenone-
639 derived SST records from relatively warm settings will have been less affected than those from
640 colder settings [e.g., *Rodrigo-Gámiz et al.*, 2016].

641 Second, the extent of degradation exerts a very strong control on SST reconstructions.
642 The *Müller et al.* [1998] SST calibration is characterized by a standard error of ± 1.5 °C, and
643 preferential $C_{37:3}$ degradation that produces biases > 1.5 °C are thus of particular concern.
644 Although previous studies argued that $\Delta\text{SST} > 1.5$ °C warm biases do occur [*Madureira et al.*,
645 1995; *Hoefs et al.*, 1998; *Gong and Hollander*, 1999; *Pagani et al.*, 1999], model results show
646 that if the extent of alkenone degradation is low ($< 50\%$), such biases require a high preferential
647 degradation factor, i.e. $f_{C37:3} \geq 1.5$ (Figure 11). This scenario seems unrealistic since it assumes
648 a $C_{37:3}$ degradation rate that is at least 50% faster than $C_{37:2}$. It is also inconsistent with most
649 experimental and field investigations (see above). Yet, if the extent of degradation is high (50
650 to 99.9%), SST biases > 1.5 °C are simulated for $f_{C37:3}$ values ranging from 1.1 to 1.4. In the
651 most extreme degradation scenario ($> 99.9\%$), any $f_{C37:3} > 1.0$ can produce SST biases above
652 1.5 °C (Fig. 11). However, as already pointed out, such high degradation rates significantly
653 reduce alkenone concentrations, rendering the analytical determination of $U_{37}^{K'}$ ratios
654 challenging. In fact, SST biases can also arise from instrumental errors when concentrations
655 are extremely low [*Grimalt et al.*, 2000, 2001].

656 Overall and holding other factors equal, reconstructed SSTs are most biased in older
657 sediments, where the extent of degradation will be most severe for a given depositional setting.

658 Although this is valid for both scenarios, in Scenario 2 (decrease in $k_i(z)$ with burial time/depth),
659 degradation rapidly slows down in very old/deeply buried sediments and differences in SST
660 bias thus become negligible when comparing sediment layers/burial times $t \gg a_i$. Model
661 results reveal how several mathematical factors mitigate and exacerbate that effect. Assuming
662 steady state, degradation is most rapid in shallow sediments and slows with depth, an effect
663 exacerbated in Scenario 2. In contrast, the impact of degradation on $U_{37}^{K'}$ increases as
664 degradation approaches its mathematical limit (*i.e.* 100%). These two factors work in tandem.
665 Therefore, we would expect Δ SST biases to occur throughout the burial time and from the
666 entire sediment column rather than solely in deep sediments. Therefore, it is useful to evaluate
667 $U_{37}^{K'}$ -derived SST records against those based on other proxies in both recent and older sediment
668 records.

669

670 *4.2.1 Assessing potential degradation bias in recent sedimentary records*

671 In general, alkenone-derived SST estimates agree well with other SST reconstructions for
672 shallow geological time periods (< 500 kyrs), indicating that diagenetic alterations of the $U_{37}^{K'}$
673 paleothermometer are negligible. For example, $U_{37}^{K'}$ and Mg/Ca (*Globigerinoides sacculifer*)
674 SSTs estimates from the Western Equatorial Pacific (WEP) are of a similar magnitude over the
675 past 30 kyr [*de Garidel-Thoron et al., 2007*]. This was observed despite relatively low alkenone
676 concentrations and possibly extensive degradation, suggesting that preferential degradation had
677 only a minor impact (*i.e.* $f_{C37:3} \approx 1.0$). The glycerol dialkyl glycerol tetraether (GDGT)-based
678 TEX₈₆ (tetraether index of tetraethers consisting of 86 carbons) proxy [*Schouten et al., 2002*]
679 is a widely used organic paleothermometer [*e.g., Schouten et al., 2013*] which also exhibits a
680 close agreement with $U_{37}^{K'}$ -derived SSTs over shallow timescales. For example, $U_{37}^{K'}$ and TEX₈₆
681 SST estimates obtained from core tops within the Arabian Sea (NIOP905 and 74KL) match
682 modern mean annual SST values for that area [*Huguet et al., 2006*]. In the Eastern

683 Mediterranean (GeoB7702-3), $U_{37}^{K'}$ and TEX_{86} also record similar trends and absolute SST
684 values over the past 27 kyr [Castañeda *et al.*, 2010]. $U_{37}^{K'}$ and TEX_{86} -based reconstructions
685 agreed well even in depth intervals where alkenone concentrations were low, indicating that
686 even a high extent of degradation did not alter the $U_{37}^{K'}$ signal at these sites. In the Western
687 Mediterranean, Huguet *et al.* [2011] reported similar temperature trends between $U_{37}^{K'}$ and
688 TEX_{86} for the last 244 – 130 kyrs. Although, TEX_{86} absolute SST were higher than $U_{37}^{K'}$ SST,
689 the difference rarely exceeded < 3 °C, which is within both proxy calibration errors (and
690 inconsistent with the latter being biased to warm temperatures). In fact, in many cases where
691 TEX_{86} and $U_{37}^{K'}$ -derived SSTs differ, it is due to the latter being colder rather than warmer
692 [Huguet *et al.*, 2006; Castañeda *et al.*, 2010; Grauel *et al.*, 2013]; and in the few settings where
693 the opposite is observed [Lopes dos Santos *et al.*, 2010; McClymont *et al.*, 2012; Seki *et al.*,
694 2012; Li *et al.*, 2013], it is often attributed to the depth of GDGT production.

695

696 4.2.2 Assessing potential degradation bias in older sedimentary records

697 In general, inferred degradation biases have been largely limited to deep time (Miocene and
698 older) settings. For instance, the absence of tri-unsaturated alkenone in many Miocene
699 sediments from DSDP (Deep Sea Drilling Program) sites 588, 608 and 730 results in $U_{37}^{K'}$ values
700 of 1 and therefore, $SST > 28$ °C [Pagani *et al.*, 1999]. RTM results suggest that these
701 observations might indicate long-term preferential consumption of $C_{37:3}$ – and indeed alkenone
702 concentrations are low in these sediments. However, such a scenario would require extensive
703 degradation and, although mathematically possible, remains inconsistent with the lack of such
704 extensive degradation in younger settings. Therefore, we suggest, based on insights gained
705 through the model investigation, that at the DSDP sites 588, 608 and 730 Miocene SST records
706 have not been extensively affected by selective degradation and that SSTs were indeed
707 relatively high. It is worth noting that one rationale for those suggestions was the much higher

708 temperatures recorded by alkenones than by planktonic foraminifera $\delta^{18}\text{O}$. However, those
709 isotopic records have almost certainly been biased by diagenetic recrystallization [*e.g.*, *Pearson*
710 *et al.*, 2001, 2007], and these records have now been discarded [*Pagani et al.*, 2010]. This
711 illustrates some of the challenges associated with multi-proxy SST reconstructions and the
712 pitfalls of interpreting proxies with preconceived notions of relative fidelity.

713 In Paleogene sediments, more complex temperature relationships have been observed,
714 with offsets between $U_{37}^{K'}$ and foraminiferal $\delta^{18}\text{O}$ -derived SSTs ranging from 0 to 10 °C [*Pagani*
715 *et al.*, 2005; *Liu et al.*, 2009]. Again, this could be due to a long-term selective degradation of
716 alkenones or diagenetic alteration of foraminifera $\delta^{18}\text{O}$ values [*Pearson et al.*, 2001, 2007;
717 *Pagani et al.*, 2010]. Our RTM results support the latter, because such significant SST bias at
718 such high $U_{37}^{K'}$ indices is difficult to achieve without nearly complete degradative loss of the
719 alkenones.

720 Nonetheless, we do acknowledge that in some settings large SST off-sets between
721 alkenones and other proxies are observed and more difficult to explain. For example, *Weller*
722 *and Stein* [2008] observed that $U_{37}^{K'}$ -derived SSTs in the Eocene Arctic Ocean were up to 10 °C
723 higher than the TEX_{86} -derived SSTs reported by *Brinkhuis et al.* [2006]. A recent re-analysis
724 of $\text{TEX}_{86}^{\text{H}}$ -derived temperatures suggests that the offset between $\text{TEX}_{86}^{\text{H}}$ and $U_{37}^{K'}$ in deep-time
725 settings could result from a calibration bias [*Ho and Laepple*, 2016]; however, if this
726 assumption is valid that would yield higher $\text{TEX}_{86}^{\text{H}}$ SSTs. *Weller and Stein* [2008] argued that
727 the observed offset arises from the distinct ecological characteristics of alkenone and GDGT
728 producers, as they likely occupy different habitats in the water column. This seems likely
729 because model results, although showing that preferential degradation of $\text{C}_{37:3}$ can yield 10 °C
730 offsets, show that this can only happen under extreme degradation conditions.

731 The RTM approach applied here illustrates how such interpretations can be tested in
732 more than simply an *ad hoc* manner when reconstructed SSTs are perceived to be too high,

733 particularly when looking at absolute SST values, since SST differences (relative values) are
734 expected to be less biased. In particular, reconstructed SSTs should be interpreted in the
735 context of the most important factors that could potentially drive putative SST biases: the
736 presumed initial $U_{37}^{K'}(0)$ value and the extent of alkenone degradation. RTM results allow
737 exploring the robustness of relative temperature changes resulting from contrasting $U_{37}^{K'}(0)$ by
738 shifting temperature changes (higher SST shifted minimally, whereas lower SST shifted more
739 strongly).

740

741 **4. Conclusions**

742 RTM simulations show that preferential degradation of tri- over di-unsaturated C₃₇ alkenone
743 can potentially alter the original signal of the $U_{37}^{K'}$ paleothermometry and consequently produce
744 positively biased SST records. Results from a plethora of environmental and degradation
745 scenarios indicate that a combination of factors can result in a large range of possible SST
746 biases, but the greatest changes require extensive alkenone degradation. Positively biased SST
747 records are also governed by the differential degradation factor between C₃₇ alkenones ($f_{C37:3}$),
748 which based on various modern studies appears to vary between 1 and 1.5; however, these
749 extreme values seem limited to only some settings. Initial $U_{37}^{K'}(0)$ plays a secondary role on the
750 SST changes. Not all of the simulated scenarios are realistic; those that yield maximum SST
751 biases would require that alkenones be effectively removed from the sedimentary record – a
752 direct consequence of the major control exerted by the degree of degradation. However,
753 modest SST biases are associated with realistic assumptions about degradation rates, consistent
754 with environmental studies (*i.e.* in oxidised turbidites). Consequently, we caution against the
755 interpretation of $U_{37}^{K'}$ indices when alkenone concentrations are low, especially if low
756 concentrations are a direct result of extensive degradation.

757 RTM results offer a possible complementary explanation for SST off-sets between $U_{37}^{K'}$
758 and other paleotemperature proxies found in the geological record and help elucidate
759 mismatches between proxies. Additionally, it can be useful to avoid erroneous
760 paleoreconstructions and interpretations derived from $U_{37}^{K'}$ diagenetically altered signals.
761 Nevertheless, comparisons between our RTM results and the alkenone sedimentary record
762 suggest that, in general, $U_{37}^{K'}$ -SST records have not been as extensively altered as sometimes
763 assumed.

764

765

766

767

768

769

770

771

772

773

774

775

776

777

778

779

780

781

782 **Tables and figure captions**

783 **Table 1:** Selective degradation alkenones RTM components

Parameter	Description	Value/Range	Unit
C	$C_{37:2}$ or $C_{37:3}$ concentration at depth		$\mu\text{g cm}^{-3}$
C_0	$C_{37:2}$ or $C_{37:3}$ concentration at SWI	0.5 – 4.5	$\mu\text{g g}^{-1}$
k_i	Degradation rate constant	$10^{-5} - 10^{-3}$	year^{-1}
a_i	Apparent initial age	$10^{-1} - 10^4$	year
p_i	Shape parameter of alkenones distribution	$10^{-2} - 10^0$	
D_{bio}	Diffusion bioturbation coefficient	12.05; 25.06	$\text{cm}^2 \text{year}^{-1}$
ω	Burial velocity	0.16; 0.36	cm year^{-1}
ρ	Sediment density	2.5	g cm^{-3}
z	Sediment depth	0 – 25.000	cm
Z_{bio}	Bioturbation depth	10	cm
	Water depth	200; 1.000	m
$U_{37}^{K'}(0)$	$U_{37}^{K'}$ initial fractionation at SWI	0.1 – 0.9	
$f_{C37:3}$	$C_{37:3}$ preferential degradation factor	1.1 – 1.5	
SST	Sea surface temperature*	$U_{37}^{K'} = 0.033 \cdot \text{SST} + 0.044$	$^{\circ}\text{C}$
ΔSST	SST excursion or bias from SWI to depth	$\text{SST}_{\text{SWI}} - \text{SST}_{\text{Depth}}$	$^{\circ}\text{C}$

784 *Müller et al. [1998];

785

786

787

788

789

790

791

792

793

794

795

796

797

798

799

800 **Table 2.** Sea surface temperature biases and total alkenone preservation in sediments from 50 and 250 mbsf, based
 801 on different 1G RTM scenarios

k_i (year ⁻¹)	Minimum Δ SST (°C) ^a		Maximum Δ SST (°C) ^b		Fraction of alkenone preserved (%) ^b	
	200 ^c	1000 ^c	200 ^c	1000 ^c	200 ^c	1000 ^c
$1.0 \cdot 10^{-5}$	0.03	0.08	2.6	5.7	48.1	20.1
$2.5 \cdot 10^{-5}$	0.09	0.20	6.4	13.5	16.6	1.9
$5.0 \cdot 10^{-5}$	0.18	0.39	12.3	22.4	2.8	0.4
$1.0 \cdot 10^{-4}$	0.35	0.74	20.8	27.1	< 0.1	< 0.1
$1.0 \cdot 10^{-3}$	2.21	2.8	27.2	27.2	<<0.1	<<0.1

802 ^aat 50 mbsf; ^bat 250 mbsf; ^cwater depth;

803

804

805

806

807

808

809

810

811

812

813

814

815

816

817

818

819

820

821 **Table 3.** Published experimental and field derived alkenones degradation data summarizing the main preferential
 822 degradation parameters

Study	Setting	$U_{37}^{K'}$ (0)	Δ SST	Extent of degradation
Teece et al., 1998	Experimental ¹	0.74	< 1.0	85
	Experimental ²	0.59	<0.1	40
Rontani et al., 2005	Experimental ¹	0.49	~ 3.0	93
	Experimental ³	0.49	<0.1	95
Rontani et al., 2008	Experimental ¹	0.77	~ 3.0	78
McCaffrey et al., 1990	Peruvian Margin	0.7	< 0.5	30
Prahl et al., 2003	MAP - 140 ky	0.71	<0.5	86
	MAP - Late Pliocene	0.91	<0.5	95
	MAP - Early Pliocene	0.91	<0.5	98
	MAP - Late Miocene	0.94	<0.5	99
Hoefs et al., 1998	MAP - Late Pliocene	0.77	0.5	>99
	MAP - Early Pliocene	0.86	2.0	>99
	MAP - Late Miocene	0.87	0.6	>99
	MAP - Middle-late Miocene	0.92	2.5	>99
Gong and Hollander, 1999	Santa Monica Basin ⁴	0.54	2.5 - 4	60

823 ¹Oxic; ²Sulphate reduction; ³Denitrification; ⁴Oxic/Anoxic; MAP – Madeira Abyssal Plain;

824

825

826

827

828

829

830

831

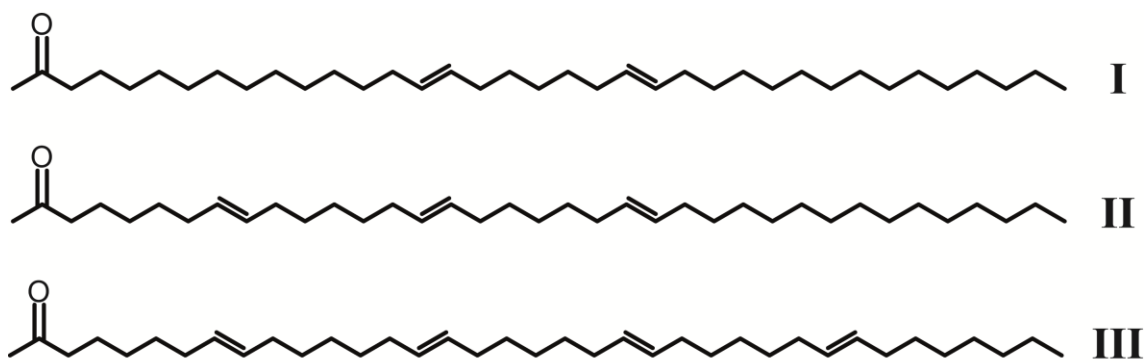
832

833

834

835

836



837

838 **Figure 1.** Chemical structure of C₃₇ alkenones. (I) Heptatriaconta-8,15-dien-2-one – C_{37:2}; (II) Heptatriaconta-

839 8,15,22-trien-2-one – C_{37:3}; (III) Heptatriaconta-8,15,22,29-tetraen-2-one – C_{37:4}.

840

841

842

843

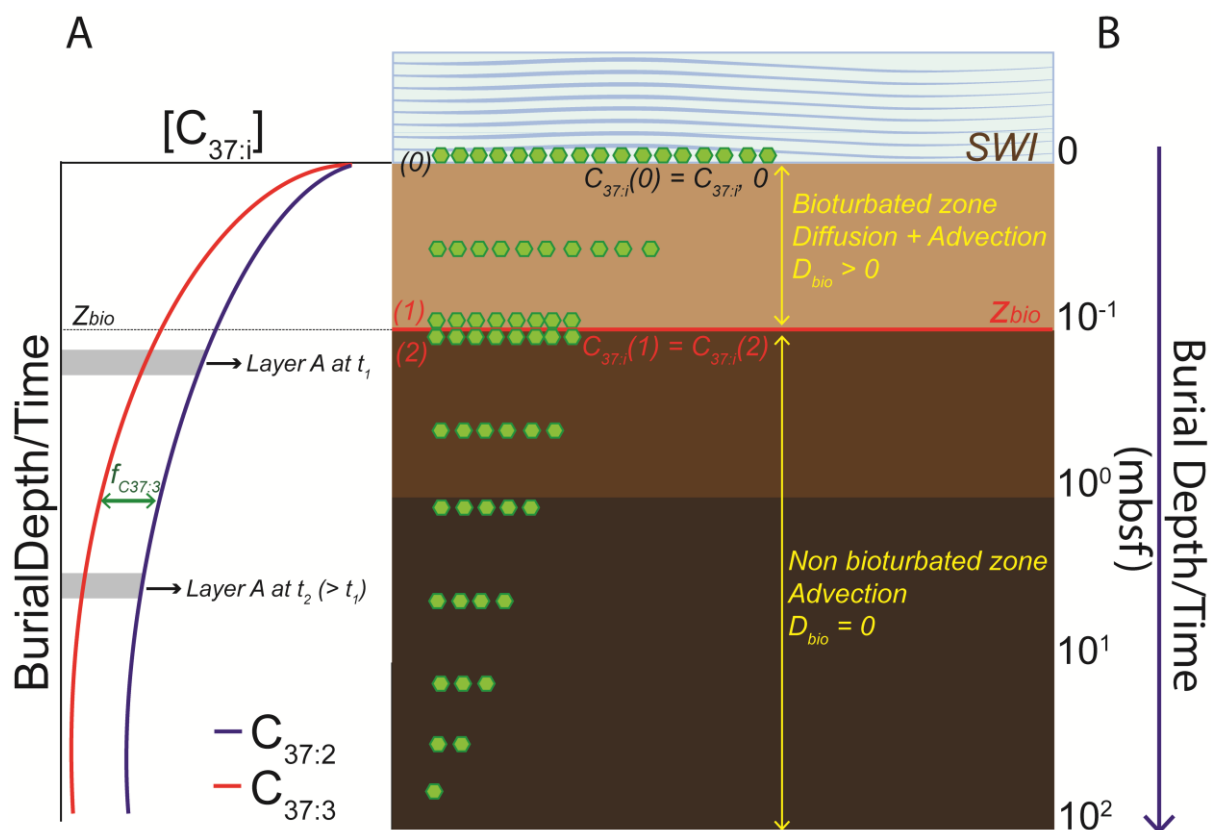
844

845

846

847

848



849

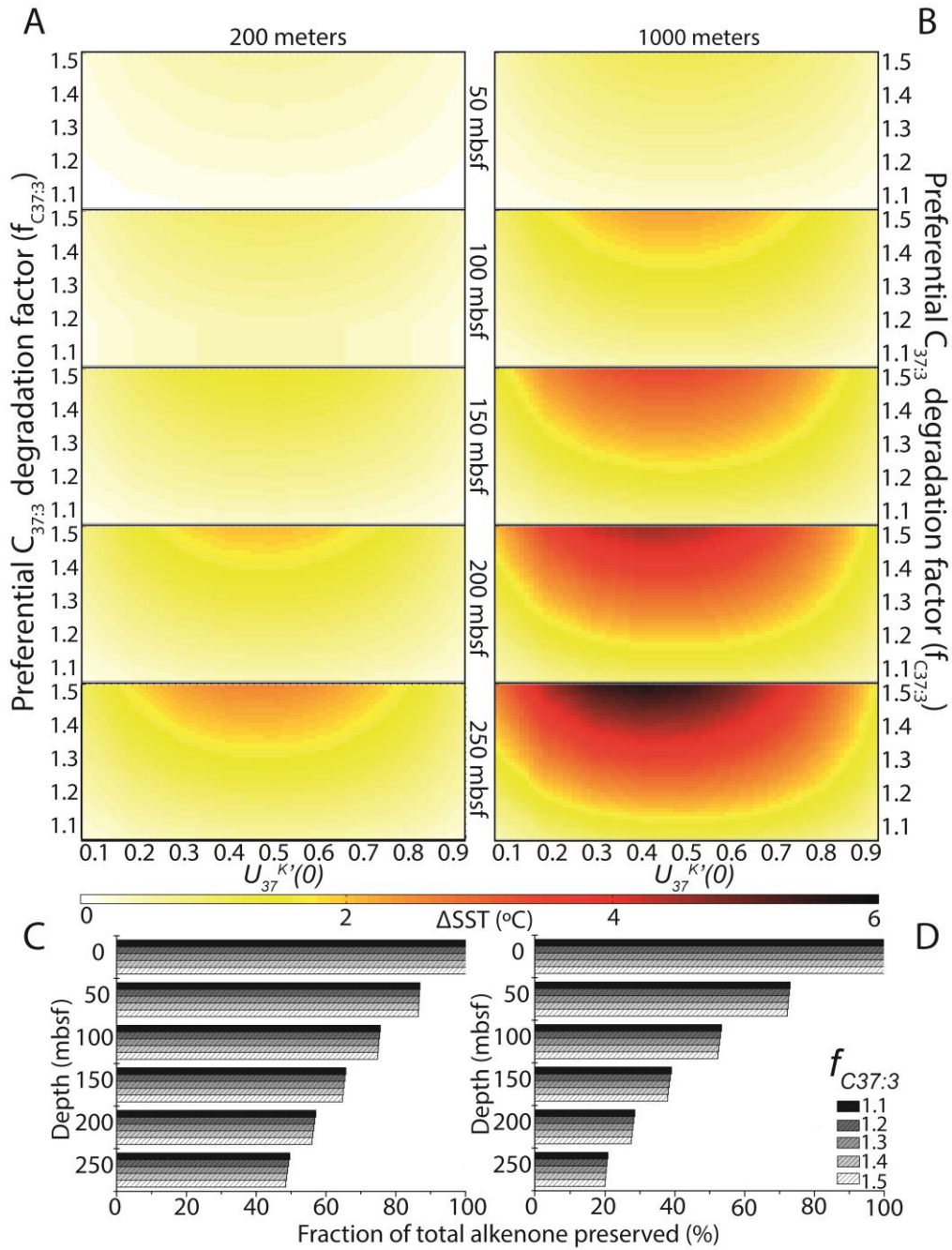
850 **Figure 2.** Schematic representation of one-dimensional alkenone degradation in marine sediments with main
 851 model elements. (a) Hypothetical downcore evolution of C_{37} alkenone concentrations ($C_{37:i}$) as a result of transport
 852 and reaction processes during burial in the sediment; the blue line represents $C_{37:2}$ alkenone concentrations,
 853 whereas the red line represents $C_{37:3}$ concentrations. The green arrow indicates the preferential degradation factor,
 854 $f_{C_{37:3}}$, of $C_{37:3}$ over $C_{37:2}$ during selective degradation. (b) Conceptual representation of C_{37} alkenone burial and
 855 degradation as a modelled sediment column; the green hexagons represent C_{37} alkenone concentrations and the
 856 red line marks the limit of bioturbated zone (Z_{bio}). D_{bio} denotes the bioturbation diffusion coefficient. SWI
 857 represents the sediment water interface.

858

859

860

861



862

863

Figure 3. Interpolated SST positive bias and total alkenones preserved in sediment resulting from selective

864

degradation of alkenones in a 1G-RTM simulation assuming a rate constant (k_i) of $1.0 \cdot 10^{-5} \text{ year}^{-1}$. (a) Downcore

865

SST bias at 200 meters water depth; (b) Downcore SST bias at 1,000 meters water depth; (c) Downcore total

866

alkenones preserved (%) in sediment at 200 meters water depth; (d) Downcore total alkenones preserved (%) in

867

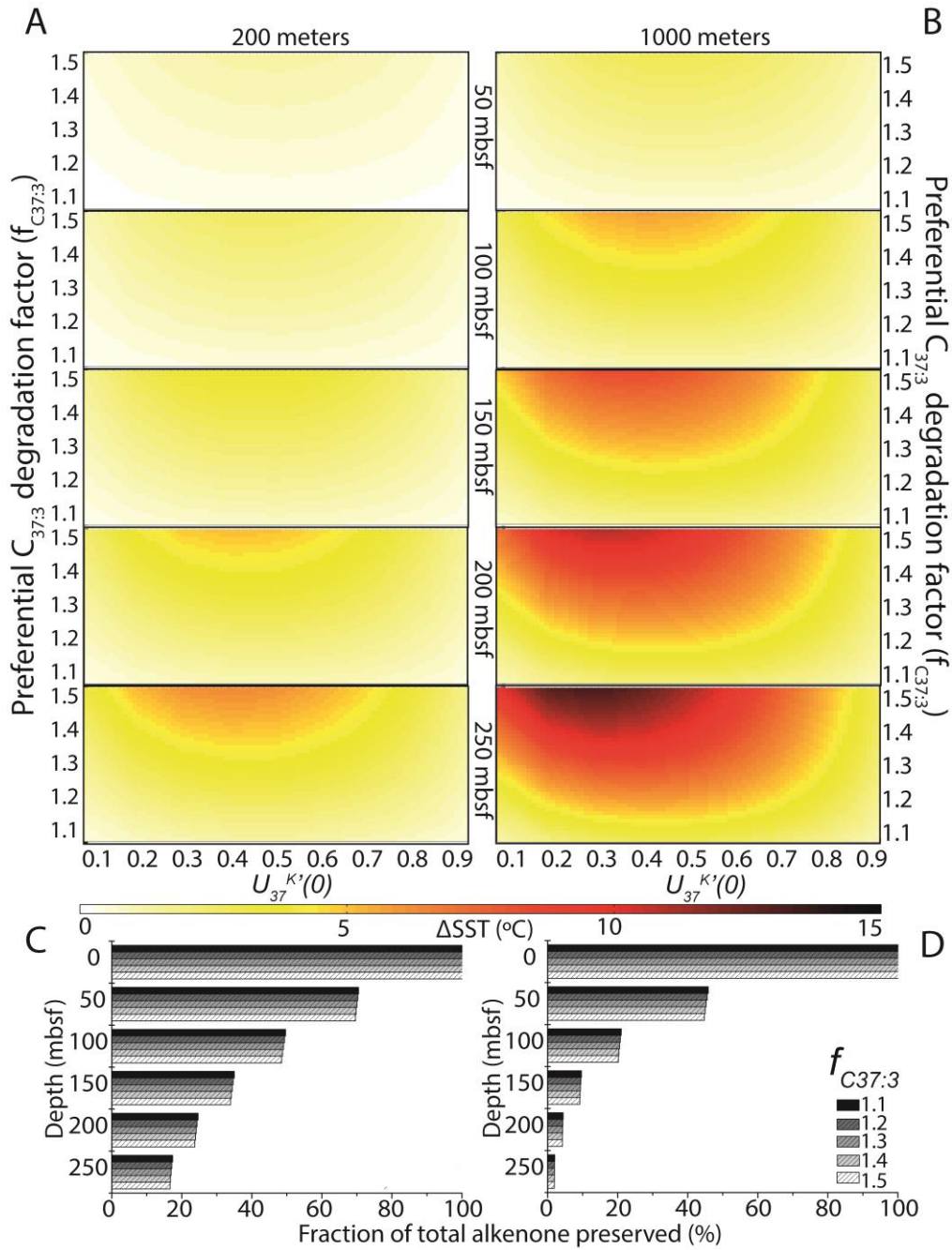
sediment at 1,000 meters water depth. ΔSST denotes SST at sediment-water interface (SWI) – SST at depth;

868

$U_{37}^{K'}(0)$ denotes $U_{37}^{K'}$ initial values at SWI; $f_{C_{37:3}}$ denotes differential degradation factor between $C_{37:3}$ and $C_{37:2}$

869

alkenones.



870

871 **Figure 4.** Interpolated SST positive bias and total alkenones preserved in sediment resulting from selective

872 degradation of alkenones in a 1G-RTM simulation assuming a rate constant (k_i) of $2.5 \cdot 10^{-5} \text{ year}^{-1}$. (a) Downcore

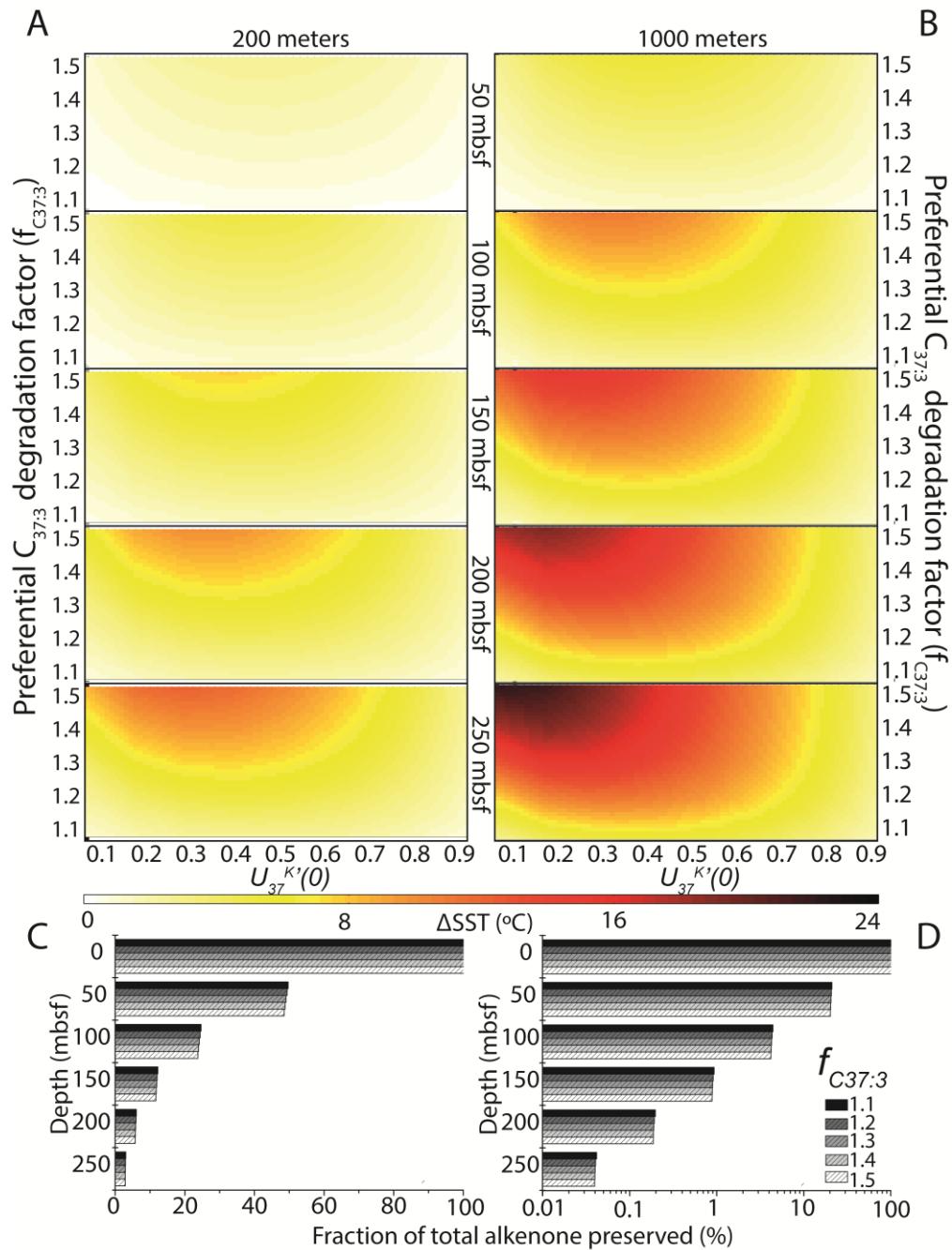
873 SST bias at 200 meters water depth; (b) Downcore SST bias at 1,000 meters water depth; (c) Downcore total

874 alkenones preserved (%) in sediment at 200 meters water depth; (d) Downcore total alkenones preserved (%) in

875 sediment at 1,000 meters water depth. ΔSST denotes SST at sediment-water interface (SWI) – SST at depth;

876 $U_{37}^{K'}(0)$ denotes $U_{37}^{K'}$ initial values at SWI; $f_{C_{37:3}}$ denotes differential degradation factor between $C_{37:3}$ and $C_{37:2}$

877 alkenones.



878

879 **Figure 5.** Interpolated SST positive bias and total alkenones preserved in sediment resulting from selective

880 degradation of alkenones in a 1G-RTM simulation assuming a rate constant (k_i) of $5.0 \cdot 10^{-5} \text{ year}^{-1}$. (a) Downcore

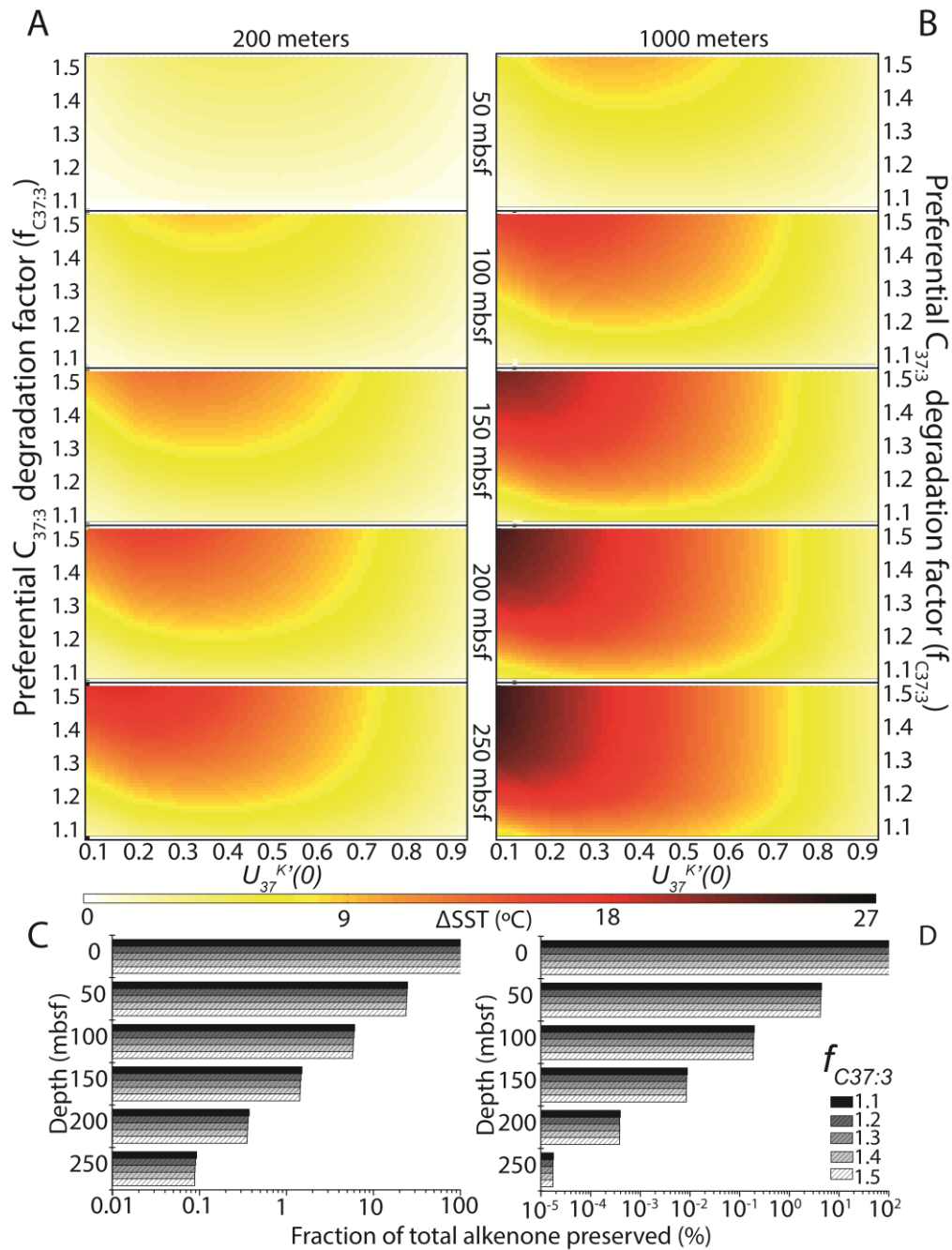
881 SST bias at 200 meters water depth; (b) Downcore SST bias at 1,000 meters water depth; (c) Downcore total

882 alkenones preserved (%) in sediment at 200 meters water depth; (d) Downcore total alkenones preserved (%) in

883 sediment at 1,000 meters water depth. ΔSST denotes SST at sediment-water interface (SWI) – SST at depth;

884 $U_{37}^{K'}(0)$ denotes $U_{37}^{K'}$ initial values at SWI; $f_{C_{37:3}}$ denotes differential degradation factor between $C_{37:3}$ and $C_{37:2}$

885 alkenones.



886

887 **Figure 6.** Interpolated SST positive bias interpolated plots and total alkenones preserved in sediment resulting

888 from selective degradation of alkenones in a 1G-RTM simulation assuming a rate constant (k_i) of $1.0 \cdot 10^{-4}$ year

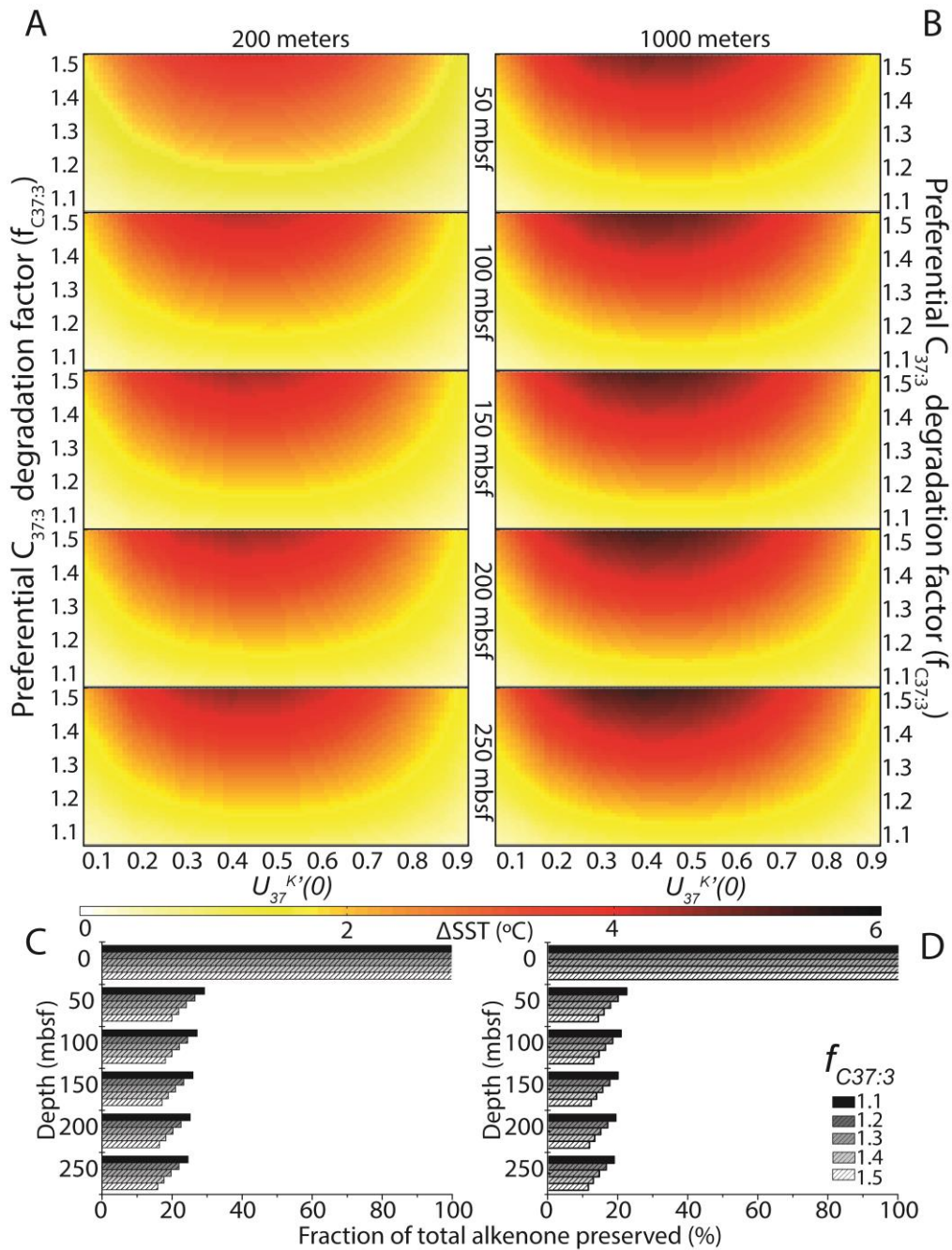
889 ¹. (a) Downcore SST bias at 200 meters water depth; (b) Downcore SST bias at 1,000 meters water depth; (c)

890 Downcore total alkenones preserved (%) in sediment at 200 meters water depth; (d) Downcore total alkenones

891 preserved (%) in sediment at 1,000 meters water depth. ΔSST denotes SST at sediment-water interface (SWI) –

892 SST at depth; $U_{37}^{K'}(0)$ denotes $U_{37}^{K'}$ initial values at SWI; $f_{C_{37:3}}$ denotes differential degradation factor between

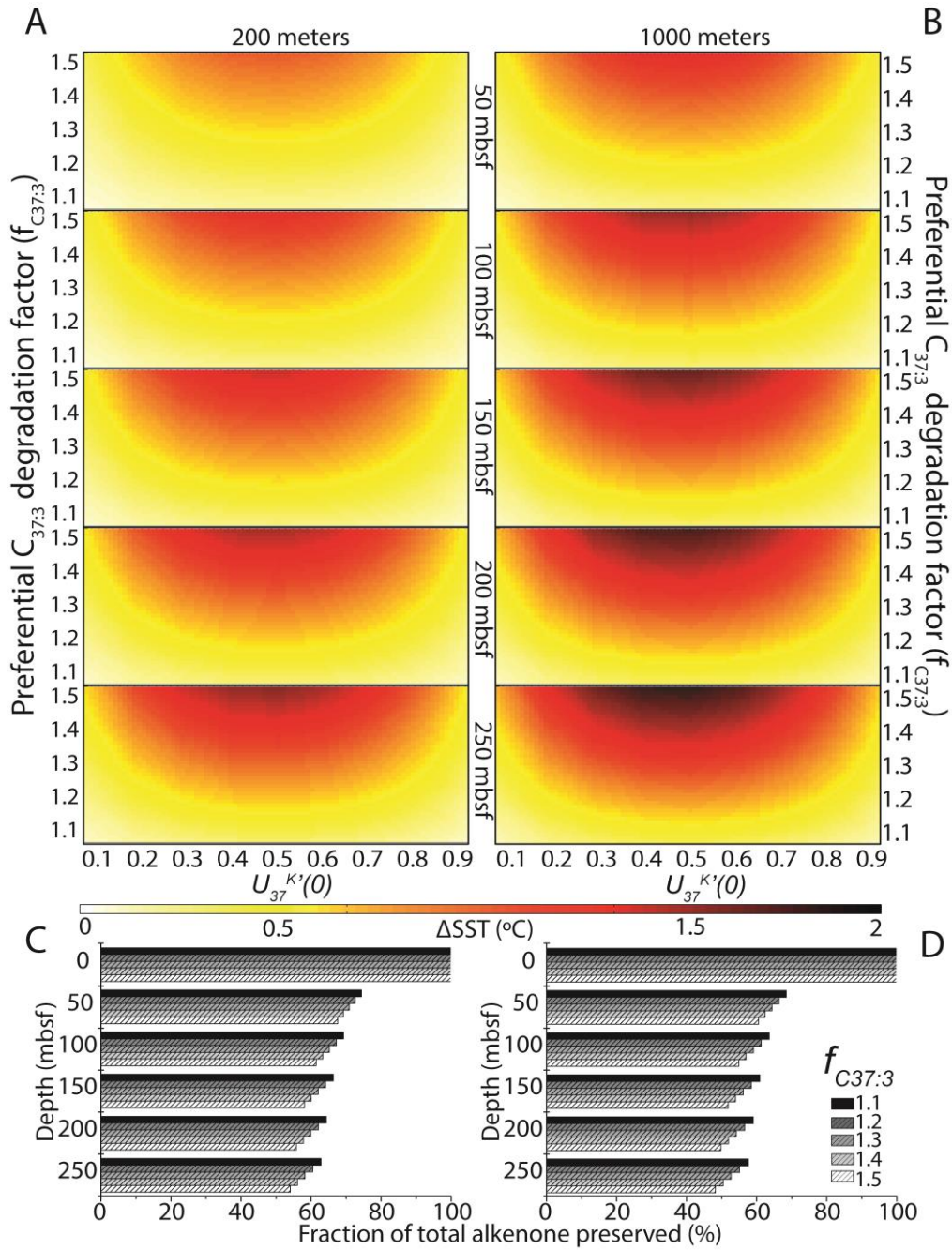
893 $C_{37:3}$ and $C_{37:2}$ alkenones.



894

895 **Figure 7.** Interpolated SST positive bias and total alkenones preserved in sediment resulting from selective
 896 degradation of alkenones in a RCM simulation assuming $p_i = 10^{-1}$ and $a_i = 10^0$ years. (a) Downcore SST bias at
 897 200 meters water depth; (b) Downcore SST bias at 1,000 meters water depth; (c) Downcore total alkenones
 898 preserved (%) in sediment at 200 meters water depth; (d) Downcore total alkenones preserved (%) in sediment at
 899 1,000 meters water depth. ΔS_{ST} denotes SST at sediment-water interface (SWI) – SST at depth; $U_{37}^{K'}(0)$ denotes
 900 $U_{37}^{K'}$ initial values at SWI; $f_{C_{37:3}}$ denotes differential degradation factor between $C_{37:3}$ and $C_{37:2}$ alkenones.

901



902

903 **Figure 8.** Interpolated SST positive bias and total alkenones preserved in sediment resulting from selective

904 degradation of alkenones in a RCM simulation assuming $pi = 10^{-1}$ and $a_i = 10^3$ years. (a) Downcore SST bias at

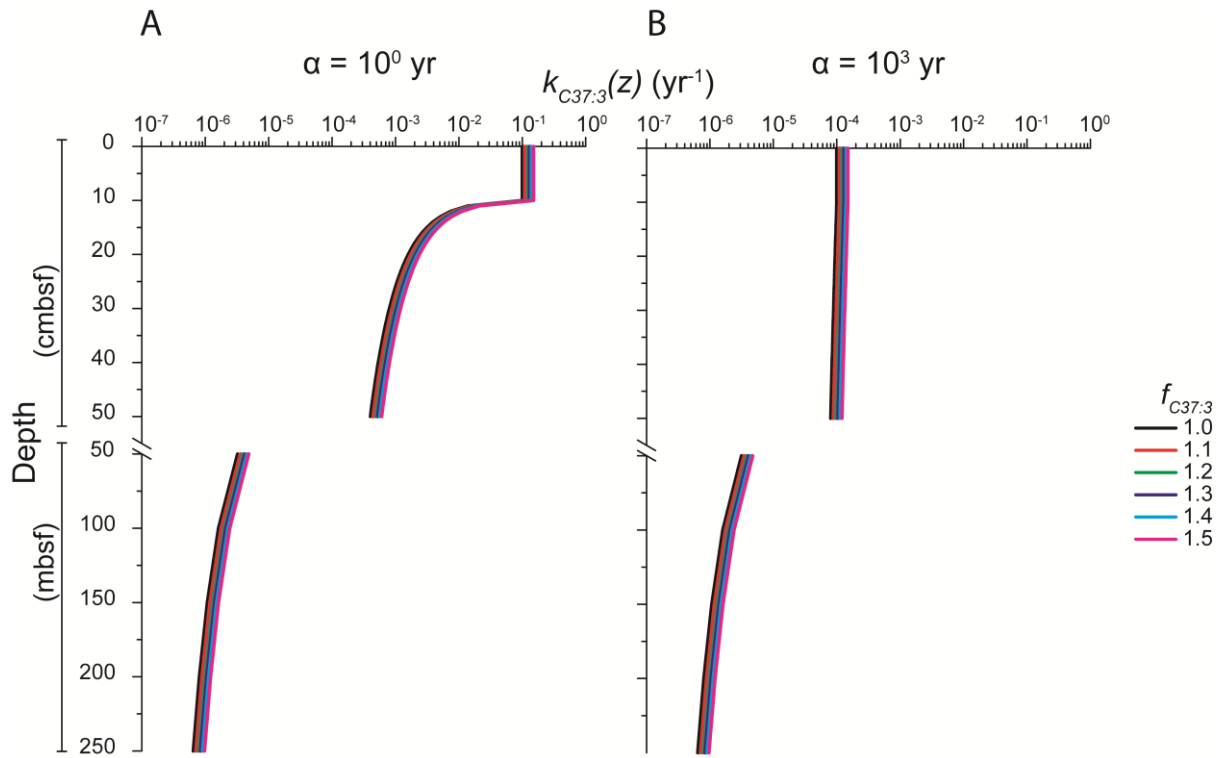
905 200 meters water depth; (b) Downcore SST bias at 1,000 meters water depth; (c) Downcore total alkenones

906 preserved (%) in sediment at 200 meters water depth; (d) Downcore total alkenones preserved (%) in sediment at

907 1,000 meters water depth. ΔSST denotes SST at sediment-water interface (SWI) – SST at depth; $U_{37}^{K'}(0)$ denotes

908 $U_{37}^{K'}$ initial values at SWI; $f_{C_{37:3}}$ denotes differential degradation factor between $C_{37:3}$ and $C_{37:2}$ alkenones.

909



910

911 **Figure 9.** Simulated downcore changes in degradation rate constant $k_{C37:3}(z)$ assuming: $p_i = 0.1$; $U_{37}^{K'}(0) = 0.5$. (a)
 912 $a_i = 10^0$ years; (b) $a_i = 10^3$ years; $f_{C37:3}$ ranges from 1.1 to 1.5 (colour lines); water depth = 1,000 meters. Note
 913 the break in scale at y-axis: top layers represent the top 50 cmbsf where the most significant changes in $k_{C37:3}(z)$
 914 and Δ SST take place; below the break, bottom layers represent the deeper sediment layers > 50 mbsf. The
 915 discontinuity in the lines is due to the break in y-axis scale.

916

917

918

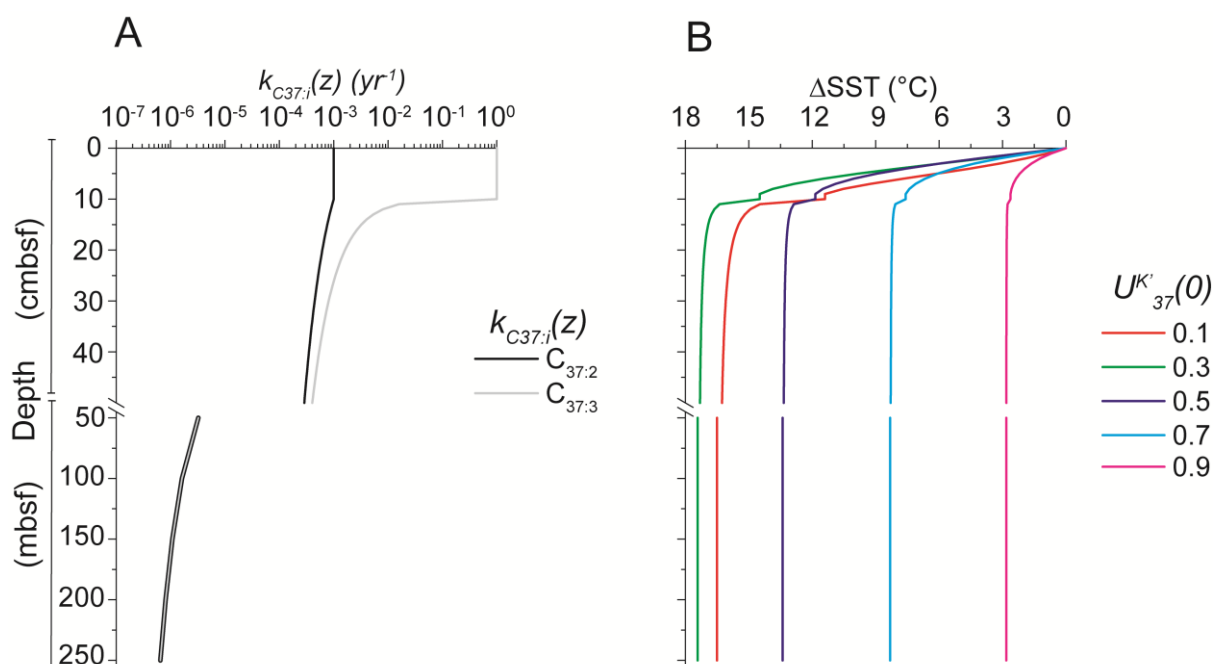
919

920

921

922

923



924

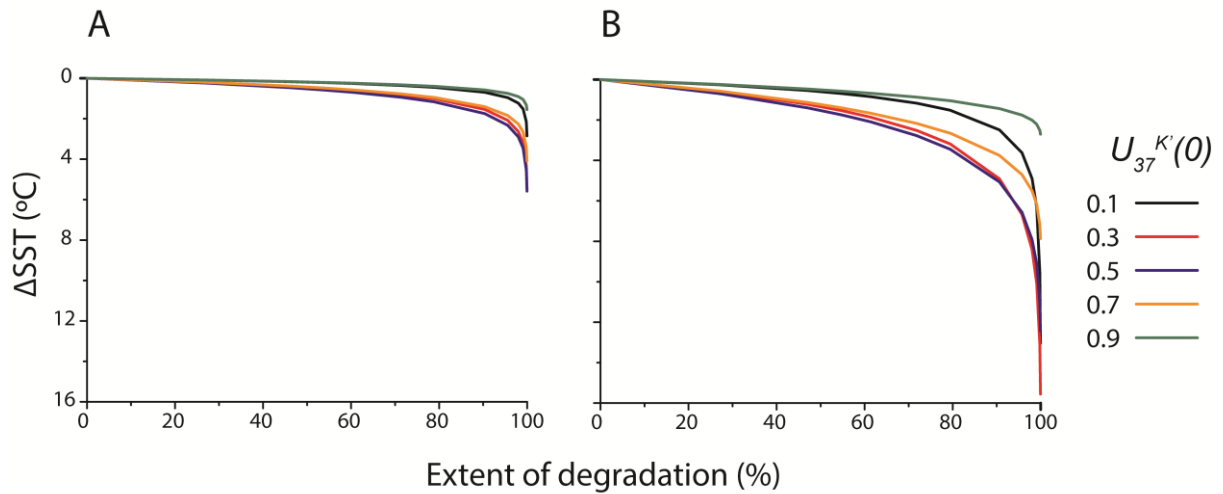
925 **Figure 10.** Simulated downcore changes in degradation rate constant $k_{C_{37:i}}(z)$ ($C_{37:2}$ black line; $C_{37:3}$ grey line) (a)
 926 and ΔSST (b) applying a power model scenario assuming: $pi = 0.1$; $a_i = 100$ years for $C_{37:2}$ (less labile pool of
 927 alkenones); $a_i = 0.1$ years for $C_{37:3}$ (more labile pool of alkenones); $U_{37}^{K'}(0)$ ranging from 0.1 to 0.9 (colour lines
 928 in B); water depth = 1,000 meters. Note the break in scale at y-axis: top layers represent the top 50 cmbsf where
 929 the most significant changes in $k_{C_{37:i}}(z)$ and ΔSST take place; below the break, bottom layers represent the deeper
 930 sediment layers > 50 mbsf. The discontinuity in the lines is due to the break in y-axis scale.

931

932

933

934



935

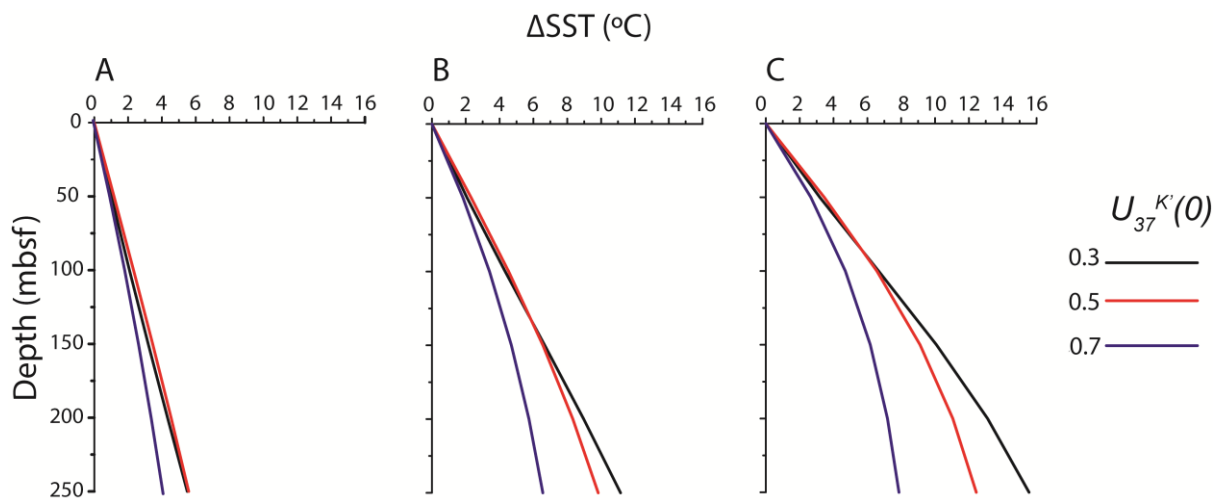
936 **Figure 11.** Increases in ΔSST with an increase in the extent of C_{37} alkenone degradation. Simulations assume: (a)

937 $f_{\text{C}37:3} = 1.1$; (b) $f_{\text{C}37:3} = 1.3$. Line colours represent $U_{37}^{K'}(0)$: black = 0.1; red = 0.3; blue = 0.5; yellow = 0.7; red =

938 0.9.

939

940



941

942 **Figure 12.** Increases in ΔSST with burial depth, assuming $k_i = 5 \cdot 10^{-5} \text{ year}^{-1}$ and 1,000 meters water depth. (a)

943 $f_{\text{C}37:3} = 1.1$; (b) $f_{\text{C}37:3} = 1.2$; (c) $f_{\text{C}37:3} = 1.3$. Line colours represent $U_{37}^{K'}(0)$: black = 0.3; red = 0.5; blue = 0.7.

944

945

946

947

948 **Acknowledgements**

949 FSF is supported by a PhD scholarship (grant number BEx 9541-13/6) from the Science
950 without Borders Programme (Ciência sem Fronteiras), sponsored by the CAPES Foundation
951 within Ministry of Education, Brazil. In addition, RDP acknowledges the advanced ERC grant
952 ‘The greenhouse earth system’ (T-GRES, project reference 340923) and the Royal Society
953 Wolfson Research Merit Award. SA acknowledges funding from the European Union’s
954 Horizon 2020 research and innovation programme under the Marie Skłodowska-Curie grant
955 agreement number 643052 745 (C-CASCADES). The authors thank Dr Jack Middelburg, Dr
956 Gordon Inglis, an anonymous reviewer, and the Associate Editor Liz Sikes for their
957 constructive comments on this manuscript. The simulated data used in this research is available
958 in tables and figures. The data derived from other studies is available in the cited references.

959

960

961

962

963

964

965

966

967

968

969

970

971 **References**

- 972 Aller, R. C. (1994), Bioturbation and remineralization of sedimentary organic matter: effects
973 of redox oscillation, *Chem. Geol.*, *114*(3-4), 331–345, doi:10.1016/0009-
974 2541(94)90062-0.
- 975 Aller, R. C., and N. E. Blair (2006), Carbon remineralization in the Amazon–Guianas tropical
976 mobile mudbelt: A sedimentary incinerator, *Cont. Shelf Res.*, *26*(17-18), 2241–2259,
977 doi:10.1016/j.csr.2006.07.016.
- 978 Arndt, S., B. B. Jørgensen, D. E. LaRowe, J. J. Middelburg, R. D. Pancost, and P. Regnier
979 (2013), Quantifying the degradation of organic matter in marine sediments: A review
980 and synthesis, *Earth-Sci. Rev.*, *123*, 53–86, doi:10.1016/j.earscirev.2013.02.008.
- 981 Arnosti, C. (2011), Microbial Extracellular Enzymes and the Marine Carbon Cycle, *Annu. Rev.*
982 *Mar. Sci.*, *3*(1), 401–425, doi:10.1146/annurev-marine-120709-142731.
- 983 Bendle, J., and A. Rosell-Melé (2004), Distributions of U_{37}^K and $U_{37}^{K'}$ in the surface waters and
984 sediments of the Nordic Seas: Implications for paleoceanography: distributions of U_{37}^K
985 and $U_{37}^{K'}$, *Geochem. Geophys. Geosystems*, *5*(11), doi:10.1029/2004GC000741.
- 986 Benthien, A., and P. J. Müller (2000), Anomalously low alkenone temperatures caused by
987 lateral particle and sediment transport in the Malvinas Current region, western
988 Argentine Basin, *Deep Sea Res. Part Oceanogr. Res. Pap.*, *47*(12), 2369–2393,
989 doi:10.1016/S0967-0637(00)00030-3.
- 990 Berner, R. A. (1980), *Early diagenesis: a theoretical approach*, Princeton series in
991 geochemistry, Princeton University Press, Princeton, N.J.
- 992 Boon, J. J., P. J. W. van der Meer, J. W. Schuyl, J. W. de Leeuw, and P. A. Schenck (1978),
993 Organic geochemical analyses of core samples from Site 362, Walvis Ridge, DSDP
994 Leg 40, in *Initial Reports of the Deep Sea Drilling Project*, vol. 38/39/40/41.
- 995 Boudreau, B. P. (1986), Mathematics of tracer mixing in sediments; II, Nonlocal mixing and
996 biological conveyor-belt phenomena, *Am. J. Sci.*, *286*(3), 199–238,
997 doi:10.2475/ajs.286.3.199.
- 998 Boudreau, B. P. (1994), Is burial velocity a master parameter for bioturbation?, *Geochim.*
999 *Cosmochim. Acta*, *58*(4), 1243–1249, doi:10.1016/0016-7037(94)90378-6.
- 1000 Boudreau, B. P. (1997), *Diagenetic models and their implementation: modelling transport and*
1001 *reactions in aquatic sediments*, Springer, Berlin ; New York.
- 1002 Boudreau, B. P. (1998), Mean mixed depth of sediments: The wherefore and the why, *Limnol.*
1003 *Oceanogr.*, *43*(3), 524–526, doi:10.4319/lo.1998.43.3.0524.
- 1004 Boudreau, B. P., and B. R. Ruddick (1991), On a reactive continuum representation of organic
1005 matter diagenesis, *Am. J. Sci.*, *291*(5), 507–538, doi:10.2475/ajs.291.5.507.
- 1006 Brassell, S. C. (2014), Climatic influences on the Paleogene evolution of alkenones,
1007 *Paleoceanography*, *29*(3), 255–272, doi:10.1002/2013PA002576.

- 1008 Brassell, S. C., and M. Dumitrescu (2004), Recognition of alkenones in a lower Aptian
1009 porcellanite from the west-central Pacific, *Org. Geochem.*, *35*(2), 181–188,
1010 doi:10.1016/j.orggeochem.2003.09.003.
- 1011 Brassell, S. C., G. Eglinton, I. T. Marlowe, U. Pflaumann, and M. Sarnthein (1986), Molecular
1012 stratigraphy: a new tool for climatic assessment, *Nature*, *320*(6058), 129–133,
1013 doi:10.1038/320129a0.
- 1014 Brinkhuis, H. et al. (2006), Episodic fresh surface waters in the Eocene Arctic Ocean, *Nature*,
1015 *441*(7093), 606–609, doi:10.1038/nature04692.
- 1016 Burdige, D. J. (2006), *Geochemistry of marine sediments*, Princeton University Press,
1017 Princeton, NJ.
- 1018 Castañeda, I. S., E. Schefuß, J. Pätzold, J. S. Sinninghe Damsté, S. Weldeab, and S. Schouten
1019 (2010), Millennial-scale sea surface temperature changes in the eastern Mediterranean
1020 (Nile River Delta region) over the last 27,000 years: Eastern Mediterranean SST
1021 records, *Paleoceanography*, *25*(1), doi:10.1029/2009PA001740.
- 1022 Conte, M. H., and G. Eglinton (1993), Alkenone and alkenoate distributions within the euphotic
1023 zone of the eastern North Atlantic: correlation with production temperature, *Deep Sea*
1024 *Res. Part Oceanogr. Res. Pap.*, *40*(10), 1935–1961, doi:10.1016/0967-0637(93)90040-
1025 A.
- 1026 Conte, M. H., G. Eglinton, and L. A. S. Madureira (1992), Long-chain alkenones and alkyl
1027 alkenoates as palaeotemperature indicators: their production, flux and early
1028 sedimentary diagenesis in the Eastern North Atlantic, *Org. Geochem.*, *19*(1-3), 287–
1029 298, doi:10.1016/0146-6380(92)90044-X.
- 1030 Cranwell, P. A., G. Eglinton, and N. Robinson (1987), Lipids of aquatic organisms as potential
1031 contributors to lacustrine sediments—II, *Org. Geochem.*, *11*(6), 513–527,
1032 doi:10.1016/0146-6380(87)90007-6.
- 1033 Farrimond, P., G. Eglinton, and S. C. Brassell (1986), Alkenones in Cretaceous black shales,
1034 Blake-Bahama Basin, western North Atlantic, *Org. Geochem.*, *10*(4-6), 897–903,
1035 doi:10.1016/S0146-6380(86)80027-4.
- 1036 Freeman, K. H., and S. G. Wakeham (1992), Variations in the distributions and isotopic
1037 composition of alkenones in Black Sea particles and sediments, *Org. Geochem.*, *19*(1-
1038 3), 277–285, doi:10.1016/0146-6380(92)90043-W.
- 1039 de Garidel-Thoron, T., Y. Rosenthal, L. Beaufort, E. Bard, C. Sonzogni, and A. C. Mix (2007),
1040 A multiproxy assessment of the western equatorial Pacific hydrography during the last
1041 30 kyr: deglacial equatorial Pacific hydrography, *Paleoceanography*, *22*(3),
1042 doi:10.1029/2006PA001269.
- 1043 Gong, C., and D. J. Hollander (1999), Evidence for differential degradation of alkenones under
1044 contrasting bottom water oxygen conditions: implication for paleotemperature
1045 reconstruction, *Geochim. Cosmochim. Acta*, *63*(3-4), 405–411, doi:10.1016/S0016-
1046 7037(98)00283-X.

- 1047 Grauel, A.-L., A. Leider, M.-L. S. Goudeau, I. A. Müller, S. M. Bernasconi, K.-U. Hinrichs,
1048 G. J. de Lange, K. A. F. Zonneveld, and G. J. M. Versteegh (2013), What do SST
1049 proxies really tell us? A high-resolution multiproxy ($U_{37}^{K'}$, TEX_{86}^H and foraminifera
1050 $\delta^{18}O$) study in the Gulf of Taranto, central Mediterranean Sea, *Quat. Sci. Rev.*, 73, 115–
1051 131, doi:10.1016/j.quascirev.2013.05.007.
- 1052 Grimalt, J. O., J. Rullkötter, M.-A. Sicre, R. Summons, J. Farrington, H. R. Harvey, M. Goñi,
1053 and K. Sawada (2000), Modifications of the C_{37} alkenone and alkenoate composition
1054 in the water column and sediment: Possible implications for sea surface temperature
1055 estimates in paleoceanography, *Geochem. Geophys. Geosystems*, 1(11),
1056 doi:10.1029/2000GC000053.
- 1057 Grimalt, J. O., E. Calvo, and C. Pelejero (2001), Sea surface paleotemperature errors in $U_{37}^{K'}$
1058 estimation due to alkenone measurements near the limit of detection,
1059 *Paleoceanography*, 16(2), 226–232, doi:10.1029/1999PA000440.
- 1060 Herbert, T. D. (2001), Review of alkenone calibrations (culture, water column, and sediments),
1061 *Geochem. Geophys. Geosystems*, 2(2), doi:10.1029/2000GC000055.
- 1062 Hoefs, M. J. L., G. J. M. Versteegh, W. I. C. Rijpstra, J. W. de Leeuw, and J. S. S. Damsté
1063 (1998), Postdepositional oxic degradation of alkenones: Implications for the
1064 measurement of palaeo sea surface temperatures, *Paleoceanography*, 13(1), 42–49,
1065 doi:10.1029/97PA02893.
- 1066 Ho, S. L., and T. Laepple (2016), Flat meridional temperature gradient in the early Eocene in
1067 the subsurface rather than surface ocean, *Nat. Geosci.*, 9(8), 606–610,
1068 doi:10.1038/ngeo2763.
- 1069 Ho, S. L., B. D. A. Naafs, and F. Lamy (2013), Alkenone paleothermometry based in the
1070 Haptophyte Algae, in *The Encyclopedia of Quaternary Science*, vol. 2, pp. 755–764,
1071 Elsevier.
- 1072 Huguet, C., J.-H. Kim, J. S. Sinninghe Damsté, and S. Schouten (2006), Reconstruction of sea
1073 surface temperature variations in the Arabian Sea over the last 23 kyr using organic
1074 proxies (TEX_{86} and $U_{37}^{K'}$): SST variations in the Arabian Sea, *Paleoceanography*, 21(3),
1075 n/a–n/a, doi:10.1029/2005PA001215.
- 1076 Huguet, C., J.-H. Kim, G. J. de Lange, J. S. Sinninghe Damsté, and S. Schouten (2009), Effects
1077 of long term oxic degradation on the TEX_{86} and BIT organic proxies, *Org. Geochem.*,
1078 40(12), 1188–1194, doi:10.1016/j.orggeochem.2009.09.003.
- 1079 Huguet, C., B. Martrat, J. O. Grimalt, J. S. Sinninghe Damsté, and S. Schouten (2011),
1080 Coherent millennial-scale patterns in $U_{37}^{K'}$ and TEX_{86}^H temperature records during the
1081 penultimate interglacial-to-glacial cycle in the western Mediterranean: $U_{37}^{K'}$ and TEX_{86}^H
1082 paleothermometry, *Paleoceanography*, 26(2), doi:10.1029/2010PA002048.
- 1083 Keil, R. G., A. F. Dickens, T. Arnarson, B. L. Nunn, and A. H. Devol (2004), What is the
1084 oxygen exposure time of laterally transported organic matter along the Washington
1085 margin?, *Mar. Chem.*, 92(1-4), 157–165, doi:10.1016/j.marchem.2004.06.024.

- 1086 de Leeuw, J. W., F. W. v.d. Meer, W. I. C. Rijpstra, and P. A. Schenck (1980), On the
1087 occurrence and structural identification of long chain unsaturated ketones and
1088 hydrocarbons in sediments, *Phys. Chem. Earth*, 12, 211–217, doi:10.1016/0079-
1089 1946(79)90105-8.
- 1090 Li, D., M. Zhao, J. Tian, and L. Li (2013), Comparison and implication of TEX86 and U37K'
1091 temperature records over the last 356kyr of ODP Site 1147 from the northern South
1092 China Sea, *Palaeogeogr. Palaeoclimatol. Palaeoecol.*, 376, 213–223,
1093 doi:10.1016/j.palaeo.2013.02.031.
- 1094 Liu, Z., M. Pagani, D. Zinniker, R. DeConto, M. Huber, H. Brinkhuis, S. R. Shah, R. M. Leckie,
1095 and A. Pearson (2009), Global Cooling During the Eocene-Oligocene Climate
1096 Transition, *Science*, 323(5918), 1187–1190, doi:10.1126/science.1166368.
- 1097 Lopes dos Santos, R. A., M. Prange, I. S. Castañeda, E. Schefuß, S. Mulitza, M. Schulz, E. M.
1098 Niedermeyer, J. S. Sinninghe Damsté, and S. Schouten (2010), Glacial–interglacial
1099 variability in Atlantic meridional overturning circulation and thermocline adjustments
1100 in the tropical North Atlantic, *Earth Planet. Sci. Lett.*, 300(3-4), 407–414,
1101 doi:10.1016/j.epsl.2010.10.030.
- 1102 Lyle, M., F. G. Prahl, and M. A. Sparrow (2006), Data report: Reconnaissance of organic
1103 biomarkers in Leg 199 sediments, in *Proceedings of the Ocean Drilling Program,*
1104 *Scientific Results*.
- 1105 Madureira, L. A. S., M. H. Conte, and G. Eglinton (1995), Early diagenesis of lipid biomarker
1106 compounds in North Atlantic sediments, *Paleoceanography*, 10(3), 627–642,
1107 doi:10.1029/94PA03299.
- 1108 Marlowe, I. T., S. C. Brassell, G. Eglinton, and J. C. Green (1984), Long chain unsaturated
1109 ketones and esters in living algae and marine sediments, *Org. Geochem.*, 6, 135–141,
1110 doi:10.1016/0146-6380(84)90034-2.
- 1111 Marlowe, I. T., S. C. Brassell, G. Eglinton, and J. C. Green (1990), Long-chain alkenones and
1112 alkyl alkenoates and the fossil coccolith record of marine sediments, *Chem. Geol.*, 88(3-
1113 4), 349–375, doi:10.1016/0009-2541(90)90098-R.
- 1114 Mayer, L. M. (1995), Sedimentary organic matter preservation: an assessment and speculative
1115 synthesis—a comment, *Mar. Chem.*, 49(2-3), 123–126, doi:10.1016/0304-
1116 4203(95)00011-F.
- 1117 McCaffrey, M. A., J. W. Farrington, and D. J. Repeta (1990), The organic geochemistry of
1118 Peru margin surface sediments: I. A comparison of the C37 alkenone and historical El
1119 Niño records, *Geochim. Cosmochim. Acta*, 54(6), 1671–1682, doi:10.1016/0016-
1120 7037(90)90399-6.
- 1121 McClymont, E. L., R. S. Ganeshram, L. E. Pichevin, H. M. Talbot, B. E. van Dongen, R. C.
1122 Thunell, A. M. Haywood, J. S. Singarayer, and P. J. Valdes (2012), Sea-surface
1123 temperature records of Termination 1 in the Gulf of California: Challenges for seasonal
1124 and interannual analogues of tropical Pacific climate change: Gulf of California
1125 Termination 1, *Paleoceanography*, 27(2), doi:10.1029/2011PA002226.

- 1126 Mercer, J. L., and M. Zhao (2004), Alkenone stratigraphy on the Northern South China Sea for
1127 the past 35 m.y., sites 1147 and 1148, ODP Leg 181, in *Proceedings of the Ocean*
1128 *Drilling Program, Scientific Results*, vol. 184.
- 1129 Middelburg, J. J. (1989), A simple rate model for organic matter decomposition in marine
1130 sediments, *Geochim. Cosmochim. Acta*, 53(7), 1577–1581, doi:10.1016/0016-
1131 7037(89)90239-1.
- 1132 Middelburg, J. J., K. Soetaert, and P. M. J. Herman (1997), Empirical relationships for use in
1133 global diagenetic models, *Deep Sea Res. Part Oceanogr. Res. Pap.*, 44(2), 327–344,
1134 doi:10.1016/S0967-0637(96)00101-X.
- 1135 Mollenhauer, G., T. Eglinton, N. Ohkouchi, R. Schneider, P. Müller, P. Grootes, and J.
1136 Rullkötter (2003), Asynchronous alkenone and foraminifera records from the Benguela
1137 Upwelling System, *Geochim. Cosmochim. Acta*, 67(12), 2157–2171,
1138 doi:10.1016/S0016-7037(03)00168-6.
- 1139 Müller, P. J., and G. Fischer (2001), A 4-year sediment trap record of alkenones from the
1140 filamentous upwelling region off Cape Blanc, NW Africa and a comparison with
1141 distributions in underlying sediments, *Deep Sea Res. Part Oceanogr. Res. Pap.*, 48(8),
1142 1877–1903, doi:10.1016/S0967-0637(00)00109-6.
- 1143 Müller, P. J., G. Kirst, G. Ruhland, I. von Storch, and A. Rosell-Melé (1998), Calibration of
1144 the alkenone paleotemperature index $U_{37}^{K'}$ based on core-tops from the eastern South
1145 Atlantic and the global ocean (60°N–60°S), *Geochim. Cosmochim. Acta*, 62(10), 1757–
1146 1772, doi:10.1016/S0016-7037(98)00097-0.
- 1147 Ohkouchi, N., T. I. Eglinton, L. D. Keigwin, and J. Hayes (2002), Spatial and Temporal
1148 Offsets Between Proxy Records in a Sediment Drift, *Science*, 298(5596), 1224–1227,
1149 doi:10.1126/science.1075287.
- 1150 Pagani, M., M. A. Arthur, and K. H. Freeman (1999), Miocene evolution of atmospheric carbon
1151 dioxide, *Paleoceanography*, 14(3), 273–292, doi:10.1029/1999PA900006.
- 1152 Pagani, M., M. A. Arthur, and K. H. Freeman (2000), Variations in Miocene phytoplankton
1153 growth rates in the southwest Atlantic: Evidence for changes in ocean circulation,
1154 *Paleoceanography*, 15(5), 486–496, doi:10.1029/1999PA000484.
- 1155 Pagani, M., J. C. Zachos, K. H. Freeman, B. Tipple, and S. Bohaty (2005), Marked Decline in
1156 Atmospheric Carbon Dioxide Concentrations During the Paleogene, *Science*,
1157 309(5734), 600–603, doi:10.1126/science.1110063.
- 1158 Pagani, M., Z. Liu, J. LaRiviere, and A. C. Ravelo (2010), High Earth-system climate
1159 sensitivity determined from Pliocene carbon dioxide concentrations, *Nat. Geosci.*, 3(1),
1160 27–30, doi:10.1038/ngeo724.
- 1161 Pearson, P. N., P. W. Ditchfield, J. Singano, K. G. Harcourt-Brown, C. J. Nicholas, R. K.
1162 Olsson, N. J. Shackleton, and M. A. Hall (2001), Warm tropical sea surface
1163 temperatures in the Late Cretaceous and Eocene epochs, *Nature*, 413(6855), 481–487,
1164 doi:10.1038/35097000.

- 1165 Pearson, P. N., B. E. van Dongen, C. J. Nicholas, R. D. Pancost, S. Schouten, J. M. Singano,
1166 and B. S. Wade (2007), Stable warm tropical climate through the Eocene Epoch,
1167 *Geology*, 35(3), 211, doi:10.1130/G23175A.1.
- 1168 Prah, F., T. Herbert, S. C. Brassell, N. Ohkouchi, M. Pagani, D. Repeta, A. Rosell-Melé, and
1169 E. Sikes (2000), Status of alkenone paleothermometer calibration: Report from
1170 Working Group 3: paleothermometer calibration, *Geochem. Geophys. Geosystems*,
1171 1(11), doi:10.1029/2000GC000058.
- 1172 Prah, F., C. P. Pilska, and M. Sparrow (2001), Seasonal record for alkenones in sedimentary
1173 particles from the Gulf of Maine, *Deep Sea Res. Part Oceanogr. Res. Pap.*, 48(2), 515–
1174 528, doi:10.1016/S0967-0637(00)00057-1.
- 1175 Prah, F. G., and S. G. Wakeham (1987), Calibration of unsaturation patterns in long-chain
1176 ketone compositions for palaeotemperature assessment, *Nature*, 330(6146), 367–369,
1177 doi:10.1038/330367a0.
- 1178 Prah, F. G., L. A. Muehlhausen, and D. L. Zahnle (1988), Further evaluation of long-chain
1179 alkenones as indicators of paleoceanographic conditions, *Geochim. Cosmochim. Acta*,
1180 52(9), 2303–2310, doi:10.1016/0016-7037(88)90132-9.
- 1181 Prah, F. G., G. J. de Lange, M. Lyle, and M. A. Sparrow (1989), Post-depositional stability of
1182 long-chain alkenones under contrasting redox conditions, *Nature*, 341(6241), 434–437,
1183 doi:10.1038/341434a0.
- 1184 Prah, F. G., G. L. Cowie, G. J. De Lange, and M. A. Sparrow (2003), Selective organic matter
1185 preservation in “burn-down” turbidites on the Madeira Abyssal Plain: selective
1186 preservation, *Paleoceanography*, 18(2), doi:10.1029/2002PA000853.
- 1187 Rechka, J. A., and J. R. Maxwell (1988), Characterisation of alkenone temperature indicators
1188 in sediments and organisms, *Org. Geochem.*, 13(4-6), 727–734, doi:10.1016/0146-
1189 6380(88)90094-0.
- 1190 Rodrigo-Gámiz, M., S. W. Rampen, S. Schouten, and J. S. Sinninghe Damsté (2016), The
1191 impact of oxic degradation on long chain alkyl diol distributions in Arabian Sea surface
1192 sediments, *Org. Geochem.*, 100, 1–9, doi:10.1016/j.orggeochem.2016.07.003.
- 1193 Rontani, J.-F., and S. G. Wakeham (2008), Alteration of alkenone unsaturation ratio with depth
1194 in the Black Sea: Potential roles of stereomutation and aerobic biodegradation, *Org.*
1195 *Geochem.*, 39(9), 1259–1268, doi:10.1016/j.orggeochem.2008.06.002.
- 1196 Rontani, J.-F., P. Cuny, V. Grossi, and B. Beker (1997), Stability of long-chain alkenones in
1197 senescing cells of *Emiliana huxleyi*: effect of photochemical and aerobic microbial
1198 degradation on the alkenone unsaturation ratio (U_{37}^K), *Org. Geochem.*, 26(7-8), 503–
1199 509, doi:10.1016/S0146-6380(97)00023-5.
- 1200 Rontani, J.-F., P. Bonin, I. Jameson, and J. K. Volkman (2005), Degradation of alkenones and
1201 related compounds during oxic and anoxic incubation of the marine haptophyte
1202 *Emiliana huxleyi* with bacterial consortia isolated from microbial mats from the
1203 Camargue, France, *Org. Geochem.*, 36(4), 603–618,
1204 doi:10.1016/j.orggeochem.2004.10.010.

- 1205 Rontani, J.-F., R. Harji, S. Guasco, F. G. Prah, J. K. Volkman, N. B. Bhosle, and P. Bonin
1206 (2008), Degradation of alkenones by aerobic heterotrophic bacteria: Selective or not?,
1207 *Org. Geochem.*, 39(1), 34–51, doi:10.1016/j.orggeochem.2007.10.003.
- 1208 Rontani, J.-F., J. K. Volkman, F. G. Prah, and S. G. Wakeham (2013), Biotic and abiotic
1209 degradation of alkenones and implications for paleoproxy applications: A review, *Org.*
1210 *Geochem.*, 59, 95–113, doi:10.1016/j.orggeochem.2013.04.005.
- 1211 Rosell-Melé, A., J. Carter, and G. Eglinton (1994), Distributions of long-chain alkenones and
1212 alkyl alkenoates in marine surface sediments from the North East Atlantic, *Org.*
1213 *Geochem.*, 22(3-5), 501–509, doi:10.1016/0146-6380(94)90122-8.
- 1214 Schouten, S., E. C. Hopmans, E. Schefuß, and J. S. Sinninghe Damsté (2002), Distributional
1215 variations in marine crenarchaeotal membrane lipids: a new tool for reconstructing
1216 ancient sea water temperatures?, *Earth Planet. Sci. Lett.*, 204(1-2), 265–274,
1217 doi:10.1016/S0012-821X(02)00979-2.
- 1218 Schouten, S., J. J. Middelburg, E. C. Hopmans, and J. S. Sinninghe Damsté (2010),
1219 Fossilization and degradation of intact polar lipids in deep subsurface sediments: A
1220 theoretical approach, *Geochim. Cosmochim. Acta*, 74(13), 3806–3814,
1221 doi:10.1016/j.gca.2010.03.029.
- 1222 Schouten, S., E. C. Hopmans, and J. S. Sinninghe Damsté (2013), The organic geochemistry
1223 of glycerol dialkyl glycerol tetraether lipids: A review, *Org. Geochem.*, 54, 19–61,
1224 doi:10.1016/j.orggeochem.2012.09.006.
- 1225 Seki, O., D. N. Schmidt, S. Schouten, E. C. Hopmans, J. S. Sinninghe Damsté, and R. D.
1226 Pancost (2012), Paleoceanographic changes in the Eastern Equatorial Pacific over the
1227 last 10 Myr: paleoceanography over the past 10 myr, *Paleoceanography*, 27(3),
1228 doi:10.1029/2011PA002158.
- 1229 Sikes, E. L., and M.-A. Sicre (2002), Relationship of the tetra-unsaturated C₃₇ alkenone to
1230 salinity and temperature: Implications for paleoproxy applications: tetra-unsaturated
1231 C₃₇ alkenone, *Geochem. Geophys. Geosystems*, 3(11), 1–11,
1232 doi:10.1029/2002GC000345.
- 1233 Sikes, E. L., J. W. Farrington, and L. D. Keigwin (1991), Use of the alkenone unsaturation ratio
1234 U₃₇^K to determine past sea surface temperatures: core-top SST calibrations and
1235 methodology considerations, *Earth Planet. Sci. Lett.*, 104(1), 36–47, doi:10.1016/0012-
1236 821X(91)90235-A.
- 1237 Sikes, E. L., J. K. Volkman, L. G. Robertson, and J.-J. Pichon (1997), Alkenones and alkenes
1238 in surface waters and sediments of the Southern Ocean: Implications for
1239 paleotemperature estimation in polar regions, *Geochim. Cosmochim. Acta*, 61(7),
1240 1495–1505, doi:10.1016/S0016-7037(97)00017-3.
- 1241 Sun, M.-Y., and S. G. Wakeham (1994), Molecular evidence for degradation and preservation
1242 of organic matter in the anoxic Black Sea Basin, *Geochim. Cosmochim. Acta*, 58(16),
1243 3395–3406, doi:10.1016/0016-7037(94)90094-9.

- 1244 Teece, M. A., J. M. Getliff, J. W. Leftley, R. J. Parkes, and J. R. Maxwell (1998), Microbial
1245 degradation of the marine prymnesiophyte *Emiliana huxleyi* under oxic and anoxic
1246 conditions as a model for early diagenesis: long chain alkadienes, alkenones and alkyl
1247 alkenoates, *Org. Geochem.*, 29(4), 863–880, doi:10.1016/S0146-6380(98)00145-4.
- 1248 Volkman, J. K. (2000), Ecological and environmental factors affecting alkenone distributions
1249 in seawater and sediments: review, *Geochem. Geophys. Geosystems*, 1(9),
1250 doi:10.1029/2000GC000061.
- 1251 Volkman, J. K., G. Eglinton, E. D. S. Corner, and T. E. V. Forsberg (1980a), Long-chain
1252 alkenes and alkenones in the marine coccolithophorid *Emiliana huxleyi*,
1253 *Phytochemistry*, 19(12), 2619–2622, doi:10.1016/S0031-9422(00)83930-8.
- 1254 Volkman, J. K., G. Eglinton, E. D. S. Corner, and J. R. Sargent (1980b), Novel unsaturated
1255 straight-chain C₃₇ - C₃₉ methyl and ethyl ketones in marine sediments and a
1256 coccolithophore *Emiliana huxleyi*, *Phys. Chem. Earth*, 12, 219–227,
1257 doi:10.1016/0079-1946(79)90106-X.
- 1258 Volkman, J. K., J. W. Farrinton, R. B. Gagosian, and S. G. Wakeham (1983), Lipid
1259 composition of coastal marine sediments from Peru Upwelling Region, in *Advances in*
1260 *organic geochemistry, 1981: proceedings of the 10th International Meeting on Organic*
1261 *Geochemistry, University of Bergen, Norway, 14-18 September 1981*, p. 800, Wiley,
1262 Chichester ; New York.
- 1263 Volkman, J. K., S. M. Barrerr, S. I. Blackburn, and E. L. Sikes (1995), Alkenones in
1264 *Gephyrocapsa oceanica*: Implications for studies of paleoclimate, *Geochim.*
1265 *Cosmochim. Acta*, 59(3), 513–520, doi:10.1016/0016-7037(95)00325-T.
- 1266 Weller, P., and R. Stein (2008), Paleogene biomarker records from the central Arctic Ocean
1267 (Integrated Ocean Drilling Program Expedition 302): Organic carbon sources, anoxia,
1268 and sea surface temperature: Paleogene Central Arctic Ocean biomarker,
1269 *Paleoceanography*, 23(1), doi:10.1029/2007PA001472.
- 1270 Zabeti, N., P. Bonin, J. K. Volkman, I. D. Jameson, S. Guasco, and J.-F. Rontani (2010),
1271 Potential alteration of U₃₇^{K'} paleothermometer due to selective degradation of alkenones
1272 by marine bacteria isolated from the haptophyte *Emiliana huxleyi*: Isolation of
1273 alkenone-degrading bacteria from *E. huxleyi*, *FEMS Microbiol. Ecol.*,
1274 doi:10.1111/j.1574-6941.2010.00885.x.
- 1275 Zonneveld, K. A. F. et al. (2010), Selective preservation of organic matter in marine
1276 environments; processes and impact on the sedimentary record, *Biogeosciences*, 7(2),
1277 483–511, doi:10.5194/bg-7-483-2010.

1278